Precambrian Research 375 (2022) 106652

Contents lists available at ScienceDirect

Precambrian Research

journal homepage: www.elsevier.com/locate/precamres

A newly recognised 1860–1840 Ma tectono-magmatic domain in the North Australia Craton: Insights from the Tennant Region, East Tennant area, and the Murphy Inlier

A.D. Clark [a,*], L.J. Morrissey [b], M.P. Doublier [a], N. Kositcin [a], A. Schofield [a], R.G. Skirrow [c]

[a] Geoscience Australia, Resources Division, GPO Box 378, Canberra, ACT 2601, Australia
[b] MinEx CRC, Future Industries Institute, University of South Australia, Mawson Lakes 5095, Australia
[c] The Australian National University, Canberra, ACT 2600, Australia

ARTICLE INFO

Keywords:
North Australian Craton
Tennant Creek
Warramunga Province
Murphy Province
East Tennant
U-Pb monazite geochronology
Phase equilibria modelling

ABSTRACT

New U-Pb monazite ages from amphibolite-facies metasedimentary rocks from the Tennant Region, Murphy Inlier and intervening East Tennant area, together with existing data, reveal the presence of an 1860–1840 Ma tectono-magmatic domain over 600 km long towards the centre of the North Australian Craton. In-situ ion probe U-Pb dating of biotite-hosted monazite in amphibolite-facies schist in the Tennant Region yielded an age of 1858 ± 7 Ma, which is attributed to north–south shortening (D_1) at 1860–1855 Ma. Existing data indicate that D_1 was associated with east–west trending, upright folds and mostly low-grade, regional metamorphism (M_1) in the Tennant Region and the Murphy Inlier. The D_1 event preceded voluminous and widespread felsic magmatism between 1855 and 1845 Ma. This included the emplacement of the Tennant Creek Supersuite, as well as the Yungkulungu Formation and equivalent stratigraphy, in the Tennant Region and in East Tennant, and the Nicholson Granite and Cliffdale Volcanics in the Murphy Inlier. Newly determined monazite ages from amphibolite-facies schist from the East Tennant area and the Murphy Inlier constrain a second episode of deformation and metamorphism (D_2/M_2) to ~ 1845 Ma, coincident with the cessation of widespread magmatism. D_2 is characterised by regional southeast to northeast trending shear zones. Phase equilibria modelling reveals that peak pressure–temperature (*P–T*) conditions during M_2 in the East Tennant area were 2.8–3.3 kbar and 655–680 °C, indicating an extremely high apparent geothermal gradient (>190 °C/kbar) that was likely influenced by the preceding magmatism. Existing data indicate that D_2 also affected the Tennant Region, where it coincided with significant Cu-Au-Bi mineralisation, albeit at significantly lower *P–T* conditions (sub-greenschist facies) than in the East Tennant area. The development of the 1860–1840 Ma tectono-magmatic domain, extending from west of the Tennant Region to east of the Murphy Inlier, marks an intermediate step in the migration of tectonism in the North Australia Craton, from the Arnhem Province in the north at 1880–1860 Ma to the Aileron and Tanami provinces in the south by ca. 1830 Ma.

1. Introduction

The North Australian Craton (NAC; Fig. 1) records 1870–1840 Ma tectono-magmatism in many of its numerous and widespread Paleoproterozoic basement inliers (e.g. Ahmad and Scrimgeour, 2013; Betts et al., 2015). This tectonism is used to support multiple regional and global paleo-tectonic models, including the assembly of Columbia/Nuna (e.g. Betts et al., 2015; Payne et al., 2009; Zhao et al., 2004). However, the tectonic setting, structural configuration, geographic extent and significance of 1870–1840 Ma tectonic and magmatic activity remain subject to debate. For example, Etheridge et al. (1987) invoke ensialic orogenesis (the Barramundi Orogeny) to explain the widespread deformation, metamorphism and magmatism, whereas more recent geochronological and geochemical data are interpreted to reflect localised, diachronous tectonism driven by various configurations of convergent margins (e.g. Betts et al., 2015; Maidment et al., 2020; McDonald et al., 1997; Payne et al., 2009; Sheppard et al., 1999; Zhao and Cooper, 1992). In the most recent of these studies, Betts et al. (2015) interpret convergent margins in the west and south of the NAC at 1870–1840 Ma, whereas Maidment et al. (2020) propose a convergent

* Corresponding author.
E-mail address: andrew.clark@ga.gov.au (A.D. Clark).

https://doi.org/10.1016/j.precamres.2022.106652
Received 12 October 2021; Received in revised form 21 March 2022; Accepted 21 March 2022
Available online 8 April 2022

margin offshore of Australia's northern coastline at this time.

A limitation on our ability to unravel the dynamic 1870–1840 Ma tectonic history of the NAC is that most geochronological and tectonic studies have focused on the provinces around the craton's present-day margins, which contain more abundant outcrop of pre-1840 Ma rocks (e.g. McDonald et al., 1997; Sheppard et al., 1999; Whelan et al., 2017; Worden et al., 2008). In this context, it is noteworthy that many models depict the present-day centre of the NAC as relatively quiescent at 1870–1840 Ma (e.g. Betts et al., 2015; Fraser et al., 2008; Zhao et al., 2004). Nevertheless, 1870–1840 Ma tectonism is recorded in rocks towards the present-day centre of the NAC, including in the Tennant Region, Murphy Inlier, and East Tennant area (Fig. 2; Ahmad et al., 2013; Compston, 1995; Donnellan, 2013). Although geochronological similarities between these regions have been noted (e.g. Ahmad and Scrimgeour, 2013; Cross et al., 2020; Maidment et al., 2020) a lack of data has precluded more robust correlations of first-order (tectono-magmatic) events. Thus, an opportunity exists for understanding the 1870–1840 Ma tectonic history of this region, which would fill a significant gap in the understanding of the NAC.

This study presents new SHRIMP U-Pb monazite geochronology to constrain the timing of deformation and metamorphism in amphibolite-facies rocks from the Tennant Region, East Tennant area, and the Murphy Inlier. Phase equilibria modelling of amphibolite facies schist from the East Tennant area is used to constrain the pressure–temperature (*P–T*) conditions of metamorphism. We integrate our results with existing geochronological data, structural observations and geological relationships to identify an 1860–1840 Ma tectono-magmatic domain, over 600 km in length, within the present-day centre of the NAC. On the basis of our findings, we provide timing constraints for the interplay between sedimentation, magmatism, deformation and metamorphism within this domain. Our findings can inform future models for the tectono-magmatic evolution of the NAC, as well as global paleo-tectonic reconstructions.

2. Regional framework

The NAC encapsulates numerous Paleoproterozoic orogenic provinces across northern Australia (Fig. 1; Myers et al., 1996; Plumb, 1979). Isotopic evidence, and the presence of several Neoarchean inliers, suggests that the NAC, or its precursors, have existed as crustal entities since the formation of gneissic basement in the Neoarchean (e.g. Champion, 2013; Cross et al., 2005; Hollis et al., 2009; Whelan et al., 2014; Wyborn et al., 1987). There is remarkably little direct evidence for tectonic activity within the craton between ca. 2400 Ma and 1870 Ma, at the current level of exposure (e.g. Ahmad and Scrimgeour, 2013). The central Pine Creek Orogen preserves a shallow marine sedimentary succession (and associated felsic volcanism) deposited at ~ 2020 Ma (Worden et al., 2008; Needham et al., 1988). Felsic and mafic magmatic rocks of the Sophie Downs Suite were emplaced in the Lamboo Province at ca. 1910 Ma, and the Pine Creek Orogen, Lamboo Province and Arnhem Province record shallow-water sedimentation between ca. 1910 Ma and ca. 1870 Ma (Ahmad and Hollis, 2013; Phillips et al., 2016; Whelan et al., 2017).

2.1. 1870–1840 Ma tectonism in the NAC

The northern, eastern and western parts of the NAC, including the Pine Creek Orogen, Lamboo Province, Mount Isa Inlier and Arnhem Province (Fig. 1) record widespread magmatism and deformation between 1870 and 1850 Ma (Ahmad and Hollis, 2013; Blake et al., 2000; Neumann et al., 2009; Whelan et al., 2017). Almost all Paleoproterozoic

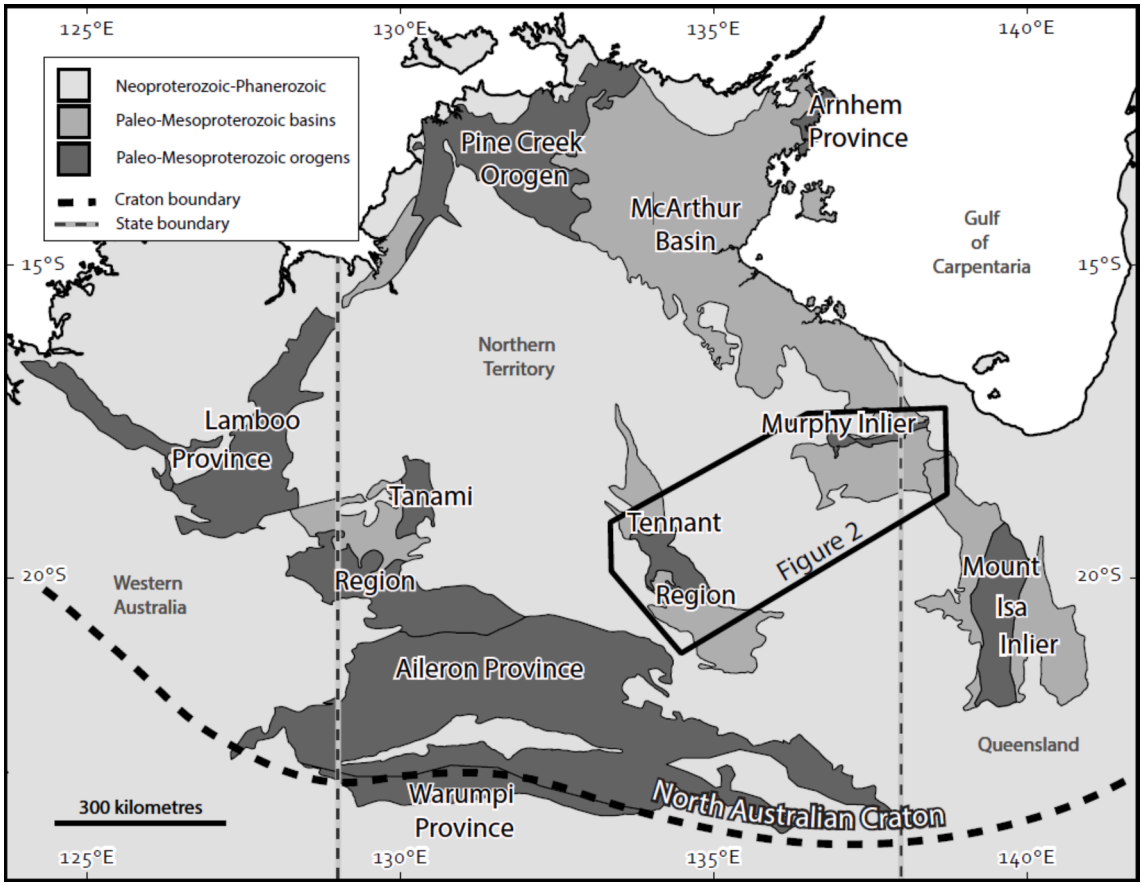

Fig. 1. Simplified map of northern Australia, showing the main areas of outcropping Paleo-Mesoproterozoic orogens that characterise the North Australia Craton. Modified after Ahmad and Scrimgeour (2013).

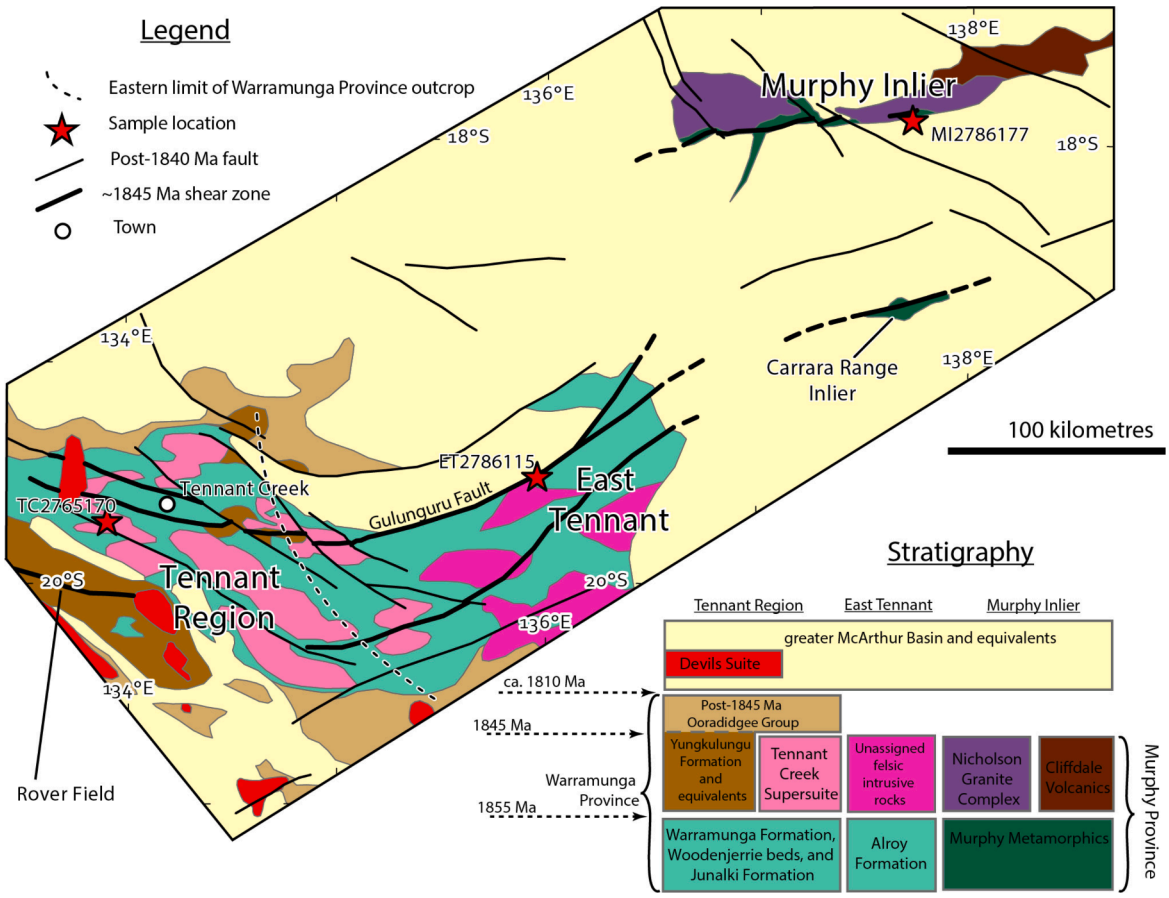

Fig. 2. Simplified geology map of the Tennant Region, East Tennant area, and Murphy Inlier. Map shows interpreted geology beneath Neoproterozoic and Phanerozoic strata, which cover much of the area. Geology modified from Stewart et al. (2020) and Clark et al. (2021b). Stars indicate locations of samples from this study.

inliers of the NAC record the deposition of turbiditic sediments within this time interval, all with remarkably similar detrital zircon age spectra and maximum deposition ages of between 1870 and 1860 Ma (e.g. Maidment et al., 2020). This suggests that a) tectono-magmatism in the craton's north and west was contemporaneous with the deposition of a widespread flysch package, and b) the craton was largely assembled prior to this time (Maidment et al., 2020).

Between 1860 and 1840 Ma, most Paleoproterozoic orogenic provinces of the NAC, with the possible exception of the Aileron Province and Tanami Region, record crustal shortening, low- to high-grade metamorphism and the emplacement of variable amounts of mostly felsic intrusive rocks (e.g. Compston, 1995; Sheppard et al., 1999; Whelan et al., 2017; Wyborn et al., 1987). Precise age data and isotopic studies have revealed that tectonism was, in part, diachronous between provinces and that some igneous rocks, e.g. the basalt in the Tickalara Metamorphics of the Lamboo Province (Sheppard et al., 1999) and the Leichardt Volcanics of the Mount Isa Inlier (McDonald et al., 1997) may have formed during convergent margin processes (e.g. Payne et al., 2009; Zhao and Cooper, 1992). This has led to numerous models for the tectonic configuration of the NAC that involve one or more convergent margins bounding the craton, and driving localised tectonism, between 1860 and 1840 Ma (e.g. Betts et al., 2015; Cawood and Korsch, 2008; Li, 2000; Maidment et al., 2020; Sheppard et al., 1999). However, as mentioned above, these models may be biased by the relative abundance of high-quality geochronological data that has been collected from the comparatively well-exposed provinces towards the craton's modern-day margins. In comparison, less is known about the timing and character of tectonism within the Murphy Inlier and the Tennant Region, which lie towards the centre of the NAC (Fig. 1).

Post-1840 Ma magmatism continued in parts of the Lamboo Province and Pine Creek Orogen (e.g. Ahmad and Hollis, 2013; Blake et al., 2000). However, after ca. 1810 Ma ductile deformation and magmatism was mostly concentrated within the southern provinces of the NAC, especially the Aileron and Tanami provinces (e.g. Scrimgeour, 2013) and the Mount Isa Inlier to the east (e.g. Betts et al., 2006). Meanwhile, most other parts of the NAC record the deposition of intracontinental basin strata (e.g. the greater McArthur Basin; Rawlings, 1999). Thus, a significant part of the NAC preserves a crustal architecture largely established prior to ~ 1840 Ma.

2.2. Tennant Region

The Tennant Region contains the only significant outcrop of pre-1840 Ma rocks between the Aileron Province and the Murphy Inlier (Fig. 1). These older rocks, which form part of the Warramunga Province, crop out around the town of Tennant Creek (Fig. 2). They are unconformably overlain to the north and south by Paleo- to Mesoproterozoic strata that belong to, or are age equivalents of, basal stratigraphy of the post-1840 Ma greater McArthur Basin (Fig. 2). Pre-1840 Ma stratigraphy in the Tennant Region is host to significant Au-Cu-Bi mineralisation around Tennant Creek and at the Rover Field (Donnellan, 2013; Skirrow and Walshe, 2002; Wedekind et al., 1989).

The oldest known supracrustal rocks in the Tennant Region include the Warramunga Formation and Woodenjerrie beds, which comprise turbiditic wacke, siltstone, and minor felsic volcanic rocks, and the Junalki Formation, which comprises volcaniclastic sedimentary rocks, tuff and lava (Donnellan et al., 1995). U-Pb zircon crystallisation and maximum deposition ages, including a crystallisation age of 1862 ± 5 Ma from felsic volcanic rocks of the Junalki Formation, constrain the age of all three units to around 1865–1860 Ma (Compston, 1995; Maidment

et al., 2006; Smith, 2001). However, the interpretation of peperitic margins of porphyries emplaced at ~ 1848 Ma has been taken to suggest that the deposition of the Warramunga Formation continued until this time (Maidment et al., 2013; McPhie, 1993). 1865–1860 Ma strata of the Tennant Region are intruded by the voluminous 1855–1845 Ma Tennant Creek Supersuite (e.g. Compston, 1995; Donnellan, 2013; Maidment et al., 2006; Maidment et al., 2013; Wyborn et al., 1998). Minor greenschist-facies aureoles have developed within ~ 100 m of some intrusions (Donnellan, 2013; Wedekind and Love, 1990).

The Warramunga Formation and its correlatives are regionally metamorphosed to lowermost greenschist-facies conditions and exhibit a characteristic early foliation that is axial planar to ~ east-trending, upright folds (e.g. Donnellan et al., 1995; Rattenbury, 1994). Intrusions of the Tennant Creek Supersuite locally cross-cut these structures, but also locally exhibit a foliation attributed to this deformation (Compston, 1995; Donnellan et al., 1995). These mutual cross-cutting relationships are interpreted to indicate that regional folding was synchronous with the emplacement of the Tennant Creek Supersuite at ~ 1855–1845 Ma (e.g. Donnellan, 2013). Several studies also recognise an episode of brittle-ductile shearing along major west- to northwest-trending shear zones that followed regional folding and was associated with Cu-Au mineralisation in the region (Nguyen et al., 1989; Hill et al., 2015; Skirrow and Walshe, 2002). Muscovite associated with this mineralisation and deformation has $^{40}Ar/^{39}Ar$ ages between ~ 1860 and 1840 Ma (Compston and McDougall, 1994; Fraser et al., 2008). Although most workers have considered the Tennant Creek Supersuite to be *syn*-tectonic with the deformation described above, and collectively refer to both the magmatism and deformation as the Tennant Event (e.g. Donnellan, 2013 and references therein), we propose that a significant amount of deformation preceded the emplacement of the Tennant Creek Supersuite (see below).

The Tennant Region also includes strata of the 1855–1810 Ma Ooradidgee Group, a shallow marine to subaerial succession of bimodal volcanic rocks and sedimentary rocks that are mostly unmetamorphosed (Donnellan, 2013, and references therein). On the basis of U-Pb age data (e.g. Smith 2001, Compston 1995), Donnellan (2013) subdivides the Ooradidgee Group into a lowermost package that contains 1855–1845 Ma strata, including the Yungkulungu and Monument formations, and two upper packages containing post-1845 Ma strata (Fig. 2). Ages obtained from drill core samples indicate that this 1855–1845 Ma volcanic package, which we refer to as the Yungkulungu Formation and equivalents, extends locally under cover to the east and southwest of Tennant Creek (Cross et al., 2020; Farias et al., 2021; Huston et al., 2020). The Yungkulungu Formation and equivalents unconformably overlie folded Warramunga Formation and correlative stratigraphy (Blake, 1984; Donnellan et al., 1995). Geochronological and geochemical data indicate that the Yungkulungu Formation and equivalents are the extrusive equivalent of the Tennant Creek Supersuite (Compston, 1995; Cross et al., 2020; Donnellan et al., 1995; Smith, 2001). This presents a contradiction for the inferred timing of magmatism and deformation during the Tennant Event, in that the Tennant Creek Supersuite is interpreted to be coeval with regional folding of strata that are unconformably overlain by the extrusive equivalent of the supersuite (i.e. the Yungkulungu Formation and equivalents) as shown in Fig. 3 (e.g. Donnellan, 2013; Maidment et al., 2013; Skirrow et al., 2019). In this study, we interpret new data to indicate that regional deformation largely predated the emplacement of the Tennant Creek Supersuite, which resolves the contradiction highlighted above.

Most rocks of the Tennant Region either contain low-grade metamorphic assemblages or are unmetamorphosed (Donnellan, 2013). However, a package of medium-grade garnetiferous paragneiss and amphibolite schist was intersected in drill core located ~ 30 km west-southwest of Tennant Creek (Bell and Hallof, 1962). These rocks are presently included within the Ooradidgee Group due to their low magnetic response relative to the Warramunga Formation, and a U-Pb zircon age of 1827 ± 9 Ma obtained from a foliated felsic rock sample (Compston, 1995; Donnellan and Johnstone, 2004). However, the textural context of this sample is not clear and, if it is an intrusive rock, it may only provide a minimum age for the surrounding supracrustal package (Compston, 1995).

2.3. East Tennant area

In the East Tennant area, which lies to the east of the Tennant Region (Clark et al., 2021a; see also Fig. 2), rocks of the Warramunga Province are completely covered by a 100–200 m thick layer of Neoproterozoic to

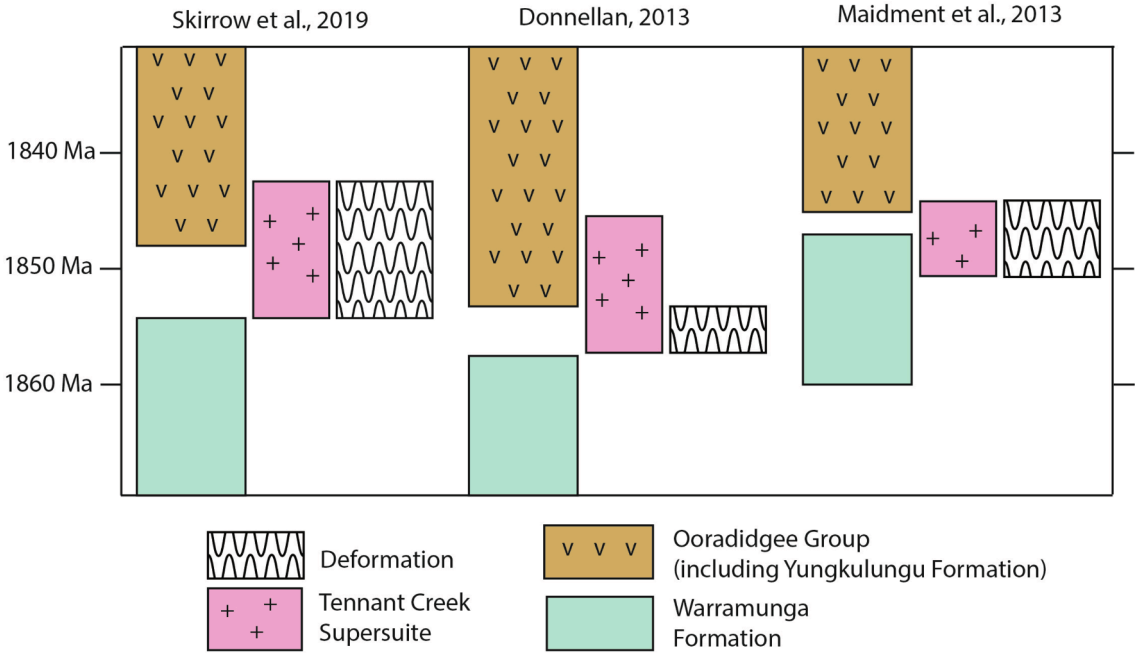

Fig. 3. Current models for the relationship between stratigraphy, magmatism and Tennant Event deformation in the Tennant region between 1870 and 1830 Ma. Summarised from Skirrow et al. (2019), Donnellan (2013), and Maidment et al. (2013).

Phanerozoic sedimentary rocks of the Georgina Basin (e.g. Walter et al., 1995). Drill core that intersects the Warramunga Province in the East Tennant area contains steeply dipping pelitic schist (locally gneissic), and subordinate marble and iron-rich rocks, termed the Alroy Formation (Clark et al., 2021a), as well as dacitic *meta*-intrusive rocks (Collins, 2009; Schofield et al., 2020; Snelling and Johnston, 1980). U-Pb zircon data indicate that intermediate intrusive rocks from the East Tennant area were emplaced at 1849 ± 3 Ma and are age equivalents of the Tennant Creek Supersuite, and that metasedimentary rocks in the East Tennant area, including the Alroy Formation, were deposited after 1872 Ma, at around the same time, or slightly earlier than, rocks of the Warramunga Formation and correlative stratigraphy in the Tennant Region (Cross et al., 2020). These data, together with a preliminary interpretation of potential field data (Clark et al., 2021b) support an affiliation between the East Tennant area and the Tennant Region. However, major uncertainties remain, especially regarding the timing and significance of deformation and metamorphism.

2.4. Murphy Inlier

The Murphy Inlier comprises pre-1800 Ma basement rocks that are unconformably overlain, and surrounded by, less deformed sedimentary rocks of the greater McArthur Basin and age-equivalent stratigraphy (Fig. 1). The basement rocks are collectively referred to as the Murphy Province (Ahmad et al., 2013). They comprise the Murphy Metamorphics, Nicholson Granite and Cliffdale Volcanics (Fig. 2). The Murphy Metamorphics consist of shale, siltstone, greywacke, schist and felsic volcanic rocks, with rare banded ironstone and calc-silicate rock (Ahmad and Wygralak, 1989; Rawlings et al., 2008). Rawlings et al. (2008) interpreted the succession as turbidity flows and chemical sediments deposited in a deep marine or shelf setting. Maximum depositional ages from this unit include 1874 ± 7 Ma (Kositcin and Carson, 2019) and 1867 ± 7 Ma (Hanley, 1996). These ages, combined with data from cross-cutting intrusive rocks of the Nicholson Granite (see below) require that protoliths of the Murphy Metamorphics were deposited at around 1860 Ma. The Murphy Metamorphics are isoclinally folded about east-trending axes and dip steeply to the north (Ahmad and Wygralak, 1989). Fold axial surfaces are sub-parallel to a foliation associated with regional, greenschist-facies metamorphism (Ahmad and Wygralak, 1989; Ahmad and Wygralak, 2014; Page et al., 2000). This deformation and metamorphism is referred to as the Murphy Event (Ahmad et al., 2013). Ahmad and Wygralak (1989) tentatively interpret a possible second tectono-metamorphic event to explain the formation of discrete shear zones within the Murphy Metamorphics, however, the timing and extent of this deformation is unknown. The Murphy Metamorphics also crop out in the small Carrara Range Inlier (Fig. 2) although the rocks there are undated (Rawlings et al., 2008).

The 1855–1845 Ma Nicholson Granite intrudes the Murphy Metamorphics and cross-cuts folding and metamorphism associated with the Murphy Event (Ahmad and Wygralak, 1989; Gardner, 1978; Kositcin et al., 2013; Page et al., 2000). The north-eastern third of the Murphy Inlier is dominated by outcrop of the flat-lying 1855–1845 Ma Cliffdale Volcanics, a succession of predominantly felsic lava and ignimbrite (Ahmad et al., 2013). Mutually cross-cutting field relationships and geochronological data indicate that the Nicholson Granite and the Cliffdale Volcanics are co-magmatic (e.g. Orth, 2009; Page et al., 2000).

3. Sample selection and petrography

In order to provide quantitative constraints on the timing and conditions of deformation and metamorphism in the Tennant Region, East Tennant area, and the Murphy Inlier, three metapelitic samples (see Fig. 2) exhibiting structural fabrics and amphibolite-facies metamorphic assemblages were selected for SHRIMP U-Pb monazite analysis and, where suitable, phase equilibria modelling. These three samples were selected following petrographic assessment of a regional sample set. Although the focus areas of this study are not well known for preserving amphibolite-facies assemblages, multiple outcrops or drill cores from each area are reported to contain medium grade rocks. Samples were selected from relatively homogeneous metamorphic assemblages in outcrop, and drill core, that are likely to extend for several kilometres, if not significantly further (see discussion below). The most pelitic samples were chosen for analysis but were taken from larger bodies of rock of equal metamorphic grade. This study is the first to report U-Pb monazite ages from the East Tennant area, the Tennant Region, or the Murphy Inlier. Therefore, our analyses should provide significant insight into the tectono-metamorphic evolution of these regions and test whether they were tectonically connected. Sample co-ordinates are given in the data table below and more detailed geological maps are provided in Appendix A.

3.1. Sample TC2765170

Sample TC2765170, a garnet schist, was chosen as a representative pelitic sample from the supracrustal package of deformed and metamorphosed basement rocks west-southwest of Tennant Creek, in the Tennant Region (see location in Fig. 2). We aimed to determine the age of tectono-metamorphism in this sample in order to establish whether its recorded tectonism was associated with the Tennant Event. This would resolve uncertainty surrounding the timing of this event and help determine whether deposition of this package of rocks might pre-date the ca. 1860 Ma Warramunga Formation. Sample TC2765170 is a subsample of a sample collected as part of Compston's (1994) PhD thesis (sample 92–231). This sample was originally obtained from a down-hole depth of 201.8–203.9 m in drill core BMR 3, hole 158 (Bell and Hallof, 1962).

Major mineral phases in sample TC2765170 include plagioclase, garnet, magnetite, quartz and biotite, which, in the absence of any obvious disequilibrium textures, are interpreted to comprise a peak metamorphic assemblage (Fig. 4A). Garnet grains are subhedral and up to 2 mm in diameter. Matrix minerals (quartz, plagioclase, magnetite, biotite) define a pervasive weak to moderate foliation that does not wrap around garnet. Aggregates of quartz commonly feature amoeboid grain boundaries and exhibit chessboard extinction, which indicates deformation at temperatures within the amphibolite facies (Fig. 4B). Monazite in sample TC2765170 is present in trace amounts throughout the matrix (mostly included in biotite) and locally within garnet grains (Fig. 5A). Monazite grains are subhedral, up to 150 μm long, weakly aligned to the pervasive foliation, and exhibit zoning in backscattered electron (BSE) imagery (e.g. Fig. 5B). There is no evidence of significant retrograde alteration in this sample, although the pervasive foliation is cross-cut by an intense but spaced foliation defined by sheared mica, quartz and magnetite, which does wrap around garnet (Fig. 4A). As a proportion of the total rock mass, any mineral regrowth associated with this younger foliation is minor.

3.2. Sample ET2786115

Sample ET2786115 was selected to provide constraints on the timing and conditions of tectono-metamorphism in the East Tennant area. This sample is a cordierite-andalusite gneiss that was obtained from a down-hole depth of 169 m in drill hole DDH005, which was drilled in 2008 by Jacaranda Minerals (Collins, 2009). It is representative of a ~ 50 m interval of steeply-dipping pelitic gneiss and schist within the Alroy Formation (Collins, 2009; Clark et al., 2021a). A sample from this interval, taken from immediately adjacent to our U-Pb monazite sample, returned a U-Pb zircon maximum deposition age of ca. 1873 Ma, which affirms the inclusion of this interval within the Alroy Formation (Cross et al., 2020).

Sample ET2786115 contains andalusite, sillimanite, biotite, muscovite, plagioclase, K-feldspar, quartz and minor cordierite (Fig. 4C). The sample exhibits subtle compositional layering defined by varying

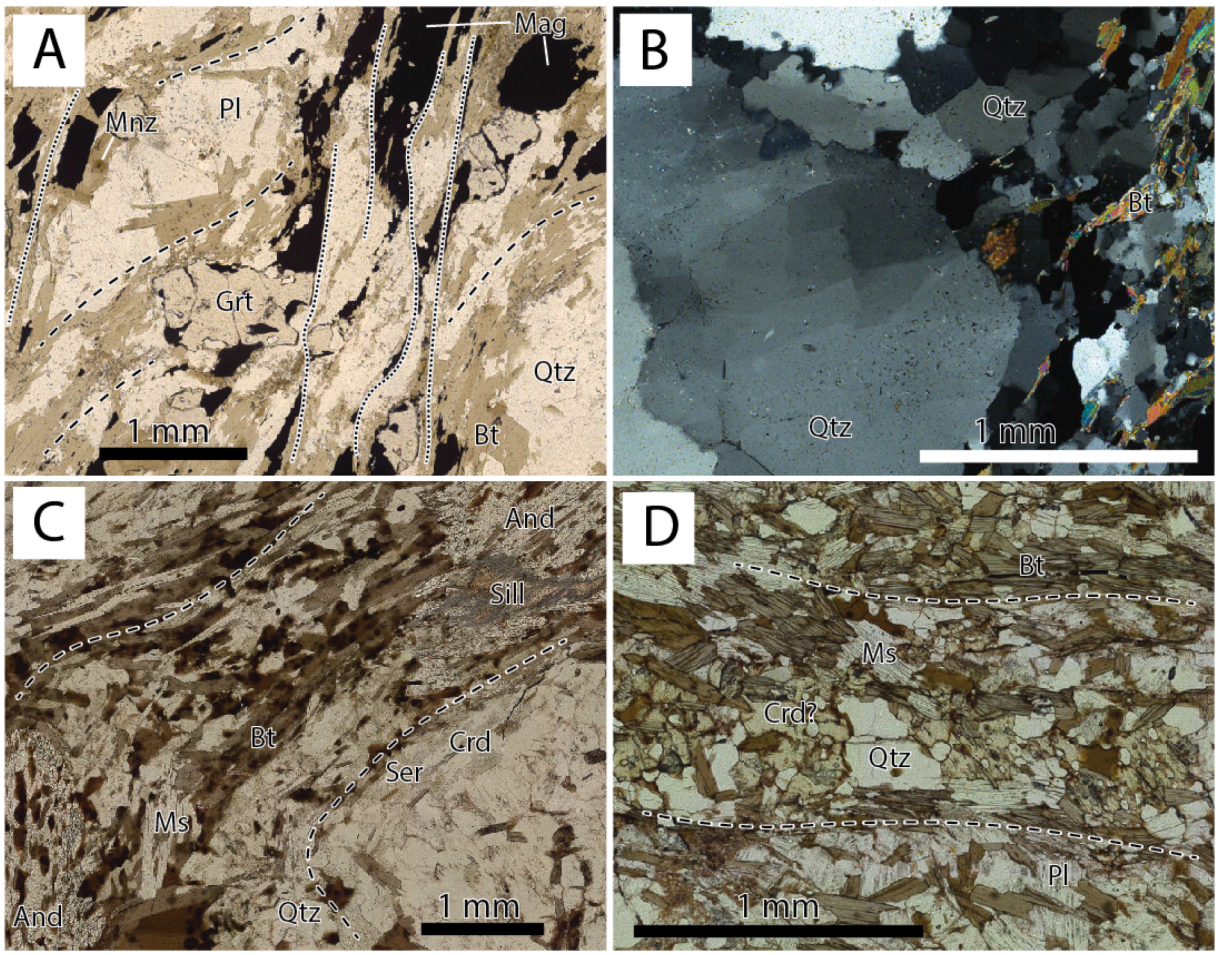

Fig. 4. Photomicrographs of samples analysed in this study. Tectonic fabric delineated by dashed (early) and dotted (late) lines. (A) Sample TC2765170 from the Tennant Region showing main mineral phases and main tectonic fabric cross-cut by younger foliation delineated by dotted lines. (B) Chessboard extinction in quartz from sample TC2765170. (C) Sample ET2786115 from the East Tennant area showing fabric defined by amphibolite-facies mineral assemblage. (D) Sample MI2786177 from the Murphy Inlier showing weak to moderate fabric defined mostly by biotite. Abbreviations: andalusite (And), biotite (Bt), cordierite (Crd), garnet, (Grt), magnetite (Mag), sericite (Ser), monazite (Mnz), muscovite (Ms), plagioclase (Pl), quartz (Qtz), sillimanite (Sill).

proportions of biotite, muscovite and quartz. Biotite and rare muscovite define a strong schistose fabric that is parallel to the compositional layering. Muscovite more commonly occurs as coarse, tabular grains that cross-cut the foliation. Biotite is also commonly included in andalusite. Andalusite (up to 5 mm in diameter) is poikiloblastic and contains inclusions of foliation-parallel biotite and quartz. Andalusite grains are surrounded by biotite and, locally, sillimanite. The modal abundance of andalusite is estimated to be approximately 1–3%. Sillimanite (fibrolite) locally overgrows but also parallels the main fabric. Sillimanite is present throughout the sample, but its abundance is heterogeneous. Its overall abundance is estimated to be around 5–10%. Rare (<3%) cordierite is aligned with the main fabric and is mostly altered to sericite. Quartz commonly exhibits amoeboid grain boundaries. Subtle chessboard extinction textures are discernible locally. Apatite and tourmaline are minor, matrix accessory phases. Monazite is present in sample ET2786115 as subhedral grains up to ~ 50 μm long that are subparallel to the main fabric (Fig. 5B, C). Most monazite is associated with biotite and sillimanite domains that show little evidence of retrograde alteration, and no monazite was observed to be included within andalusite. Monazite grains appear unzoned in BSE images (Fig. 5B).

3.3. Sample MI2786177

This sample was selected from outcrop of quartz-mica schist of the Murphy Metamorphics in order to constrain the timing of deformation and regional metamorphism in the Murphy Inlier. The sample was collected 250 m north of the southern outcrop limit of the Murphy Inlier (Fig. 2), where a well-developed foliation strikes east–west and dips steeply to the north. A sample of the Murphy Metamorphics from the same outcrop returned a maximum depositional age of 1874 ± 7 Ma (Kositcin and Carson, 2019).

Sample MI2786177 contains muscovite, quartz, microcline, plagioclase and biotite as major phases (Fig. 4D). A pale yellow mineral with a complex texture in crossed-polarised light is tentatively interpreted as weathered sericite after cordierite. Aligned micas and subtle compositional banding define a moderately-developed foliation in thin-section. Quartz, plagioclase and microcline are present throughout the sample. Monazite in sample MI2786177 is present as rounded to sub-rounded grains up to ~ 50 μm in length that are weakly aligned to the main fabric (Fig. 5D). Monazite is commonly associated with well-formed biotite and muscovite that show no evidence of retrograde alteration. Monazite in this sample exhibits little zoning in BSE imagery (Fig. 5B).

4. Analytical methods

4.1. SHRIMP U–Pb monazite geochronology

For each sample, at least two polished thin-sections were carbon coated and investigated using optical microscopy and back-scattered electron imagery acquired with Geoscience Australia's JEOL JSM-

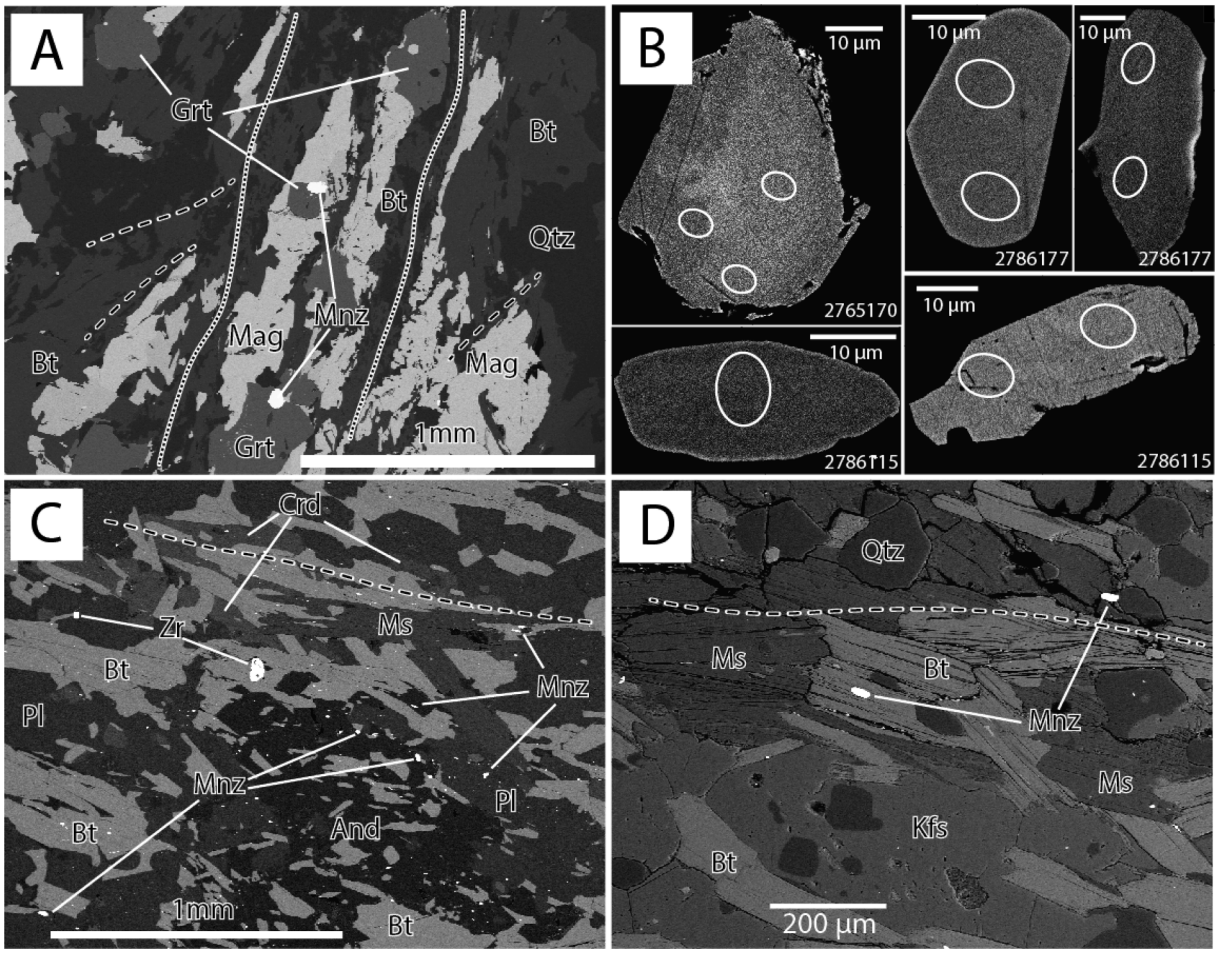

Fig. 5. Backscattered electron images of samples and monazite grains analysed in this study. Tectonic fabric delineated by dashed (early) and dotted (late) lines. (A) Backscattered electron image of Tennant Region sample (TC2765170). Note large monazite grains included within, or intergrown with, garnet. (B) Representative backscattered electron images of monazite grains from all three samples (sample numbers as labelled). (C) Backscattered electron image of East Tennant area Sample (ET2786115) showing textural location of monazite grains relative to mineral phases and tectonic fabric. Note large, rounded zircon grain. (D) Backscattered electron image of Murphy Inlier sample (MI2786177) showing monazite aligned with main tectonic fabric. Abbreviations: andalusite (And), biotite (Bt), cordierite (Crd), garnet, (Grt), magnetite (Mag), monazite (Mnz), muscovite (Ms), plagioclase (Pl), quartz (Qtz).

6490LV Scanning Electron Microscope (SEM) at an accelerating voltage of 15 keV. Five millimetre diameter cores containing suitably sized (>30 µm) and texturally relevant monazite grains were drilled from thin-sections following the method of Rayner and Stern (2002). Between seven and eight cores were obtained from each sample and, together with reference monazites (see Appendix B), were cast into three standard 25 mm SHRIMP mounts. Isotopic analyses were undertaken using the SHRIMP IIe at Geoscience Australia, Canberra.

The analytical procedures adopted for monazite analysis broadly follow those described by Stern and Sanborn (1998) and Stern and Berman (2000), and are detailed in Appendix B. Moacyr monazite GSC8153 ($^{206}Pb/^{238}U$ = 513.1 Ma; Carson et al., 2008; Fletcher et al., 2012; Palin et al., 2013) was used as the primary calibration reference material and uranium concentration standard. Monazite USGS44069 ($^{206}Pb/^{238}U$ = 424.9 Ma; Aleinikoff et al., 2006) was used as a secondary validation standard, and GSC1409 ($^{207}Pb/^{206}Pb$ = 1768.0 Ma; Stern and Berman, 2000) was used as a monitor of possible $^{207}Pb/^{206}Pb$ fractionation. Data were reduced, calculated and portrayed using Microsoft Excel® 2003, and the add-ins SQUID 2.50.11.02.03 (February 2011 revision of Ludwig, 2009) and Isoplot 3.71.09.05.23 (May 2009 revision of Ludwig, 2003). Following analysis, all monazites were examined in back-scattered electron imagery to evaluate the accuracy of SHRIMP beam placement. Analyses that were poorly targeted, >10% discordant, or affected by instrument instability were excluded.

4.2. Phase equilibria modelling

The sample of andalusite-cordierite schist from drill hole DDH005 (ET2786115) was selected for phase equilibria modelling to constrain the conditions of metamorphism. Whole rock geochemical data were generated by Bureau Veritas, Perth. The sample was powdered and fused with 4% Li nitrate to form a glass bead. Major elements were determined by X-ray fluorescence spectrometry and trace elements were analysed by Laser Ablation Mass Spectrometry. Whole rock geochemistry is presented in Appendix C.

The phase equilibria model for sample ET2786115 was calculated using THERMOCALC v3.40, using the internally consistent dataset, ds62, of Holland and Powell (2011) and activity–composition (a–x) models in the system NCKFMASHTO (Na_2O–CaO–K_2O–FeO–MgO–Al_2O_3–SiO_2–H_2O–TiO_2–Fe_2O_3; White et al., 2014). MnO was not included in the modelling to avoid artificially stabilising small amounts of garnet at lower pressures, especially given the low concentration of MnO in sample ET2786115 (0.07 wt%). The sample does not contain oxides, so a reduced oxidation state equivalent to ~ 2% of total Fe as Fe_2O_3 was selected. The H_2O content was taken as LOI, equivalent to 1.82 wt% H_2O, which allows a small amount of free H_2O to be present within the peak field. The sensitivity of the peak assemblage to variations in oxidation state and H_2O content was assessed using T–M_O and T–M_{H2O} sections calculated at 3 kbar, based on the presence of

andalusite (Appendix C). Variations in oxidation state affect the stability of oxides but do not significant change the stability fields of major silicate minerals. The peak assemblage is insensitive to the range of bulk rock H_2O contents (0.5–3 wt%) explored in the T–M_{H2O} section. Pseudosections were contoured for the modal proportion of minerals using TCInvestigator (Pearce et al., 2014).

5. Results

5.1. SHRIMP U-Pb monazite geochronology

Representative back-scattered electron (BSE) images of monazite grains and their textural locations are shown in Fig. 5. Concordia plots are shown in Fig. 6. All SHRIMP U–Pb data are provided in Table 1.

5.1.1. Sample TC2765170

Thirty-six analyses were performed on 15 monazite grains in this sample, including matrix monazite and monazite included within garnet. Two analyses were excluded due to high common Pb ($^{206}Pb_c$ > 1%), eight analyses were excluded due to discordance>10%, and another three analyses were excluded due to instrument instability. The remaining analyses form a single population with a weighted mean $^{207}Pb/^{206}Pb$ age of 1858 ± 7 Ma (95% conf., n = 23, MSWD = 1.21, probability = 0.23). Within this population, Y concentration varies from 0.09 to 2.48 wt%, U concentration varies from around 200 to 3600 ppm, and $^{232}Th/^{238}U$ varies from 10.5 to 284.5. Relatively high errors for monazite ages from this sample are attributed to low U concentrations. There is no discernible relationship between monazite age, Y concentration, zoning in backscattered electron imagery, or textural location in thin-section (including monazite included in garnet).

5.1.2. Sample ET2786115

Twenty analyses were performed on 19 monazite grains. Three analyses were excluded due to a misplaced primary beam spot and two analyses were excluded due to machine instability. The remaining analyses form a single population with a weighted mean $^{207}Pb/^{206}Pb$ age of 1844 ± 3 Ma (95% conf., n = 15, MSWD = 0.90, probability = 0.56). Within this population, Y concentration varies from around 1.46 to 1.91 wt%, U concentration varies from around 2300 to 9800 ppm, and Th/U varies from 7.0 to 14.2. There is no discernible relationship between monazite age and Y concentration.

5.1.3. Sample MI2786177

Nineteen analyses were performed on 18 monazite grains. Three analyses were excluded due to discordance above 10% and three analyses were excluded due to instrument instability. The remaining analyses form a single population with a weighted mean $^{207}Pb/^{206}Pb$ age of 1845 ± 4 Ma (95% conf., n = 13, MSWD = 0.99, probability = 0.46). Within this population, Y concentration varies from around 1.44 to 2.50 wt%, U concentration varies from around 3400 to 6000 ppm, and $^{232}Th/^{238}U$ varies from 7.1 to 12.5. There is no discernible relationship between monazite age and Y concentration.

5.2. Phase equilibria modelling

The peak assemblage in sample ET2786115 (see Fig. 7A) is interpreted to be plagioclase + K-feldspar + biotite + cordierite + sillimanite + quartz (+H_2O). Andalusite is commonly enveloped by sillimanite and biotite, and is therefore interpreted as a relic of prograde metamorphism, with sillimanite stable at peak conditions. Muscovite commonly cross-cuts the fabric and is interpreted to be retrograde. The rock contains no evidence for partial melting in hand sample or in thin section, suggesting peak temperatures were below the solidus. The interpreted peak assemblage is stable in field 6, and also in the adjacent field 8 with the addition of small amounts of ilmenite, which is not present in the rock (Fig. 7A). The relative abundance of sillimanite and

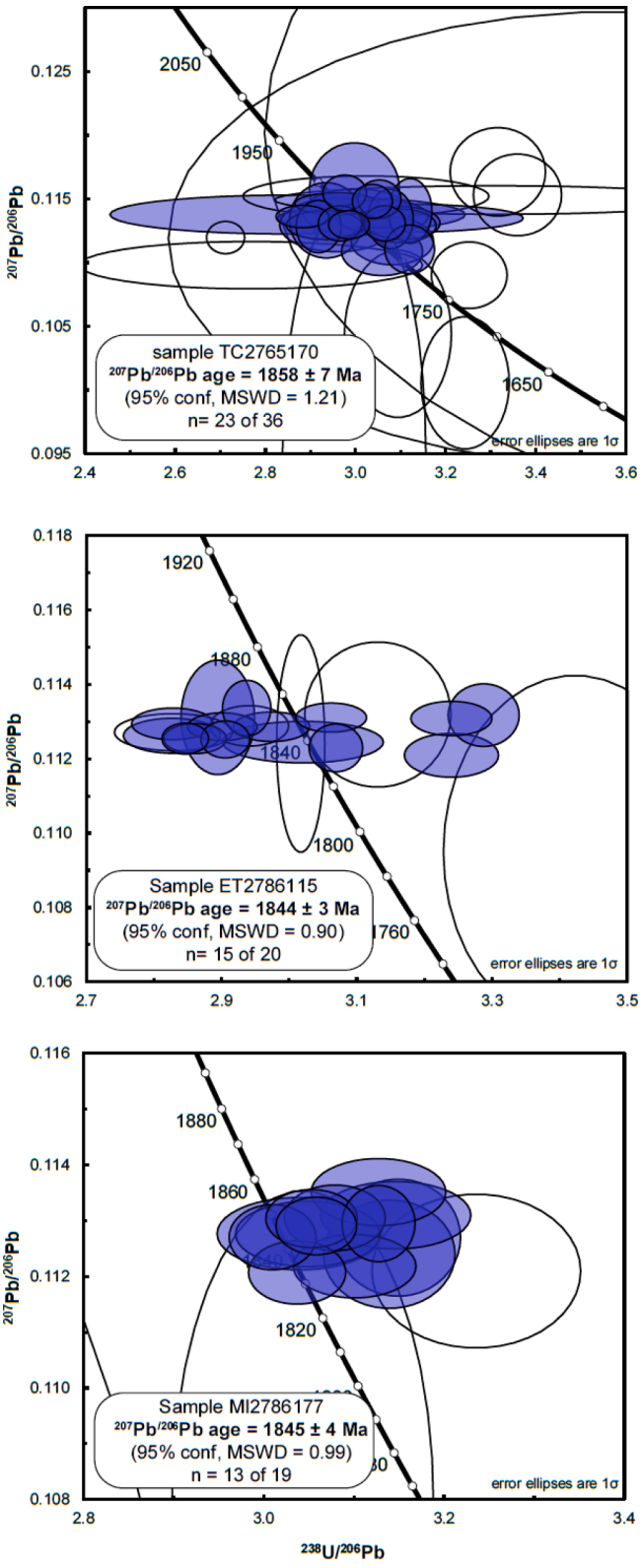

Fig. 6. Tera-Wasserburg Concordia plots for monazite age data from sample TC2765170 from the Tennant Region (top), ET2786115 from the East Tennant area (middle), and MI2786177 from the Murphy Inlier (bottom). Unfilled ellipses indicate analyses excluded from population age calculations. See text for details.

Table 1
Monazite U-Pb isotopic data from samples analysed in this study.

SampleNo.plug. grain.spot	Y (ppm)	206Pbc (%)	U (ppm)	Th (ppm)	232Th /238U	238U /206Pb	±1σ (%)	207Pb /206Pb	±1σ (%)	207Pb/206Pb Date (Ma)	±1σ (Ma)	Disc. (%)
Tennant Region (TC2765170) - GA Sample no. **2765170**; drill hole BMR3 158 (201.8–203.9 m depth), Lat −19.7198, Long 133.9036 (GDA94)												
1856 ± 7 Ma population (n = 23)												
170.D.2.1	24,811	0.00	180	49,525	284.5	2.997	2.20	0.11575	2.08	1892	37	+2
170.C.1.1	1209	0.05	1293	37,831	30.2	2.975	1.08	0.11547	0.80	1887	14	+1
170.E.3.1	3944	0.24	1315	59,429	46.7	3.052	1.04	0.11500	0.85	1880	15	+3
170.F.1.3	2241	0.44	2997	31,816	11.0	3.036	0.95	0.11479	0.76	1877	14	+3
170.C.3.1	4810	0.12	3627	65,234	18.6	2.957	2.05	0.11461	0.49	1874	9	−0
170.F.1.2	1704	0.43	2123	22,880	11.1	3.120	1.02	0.11405	1.48	1865	27	+4
170.F.1.6	5697	0.01	3122	50,401	16.7	3.001	2.61	0.11396	1.06	1864	19	+1
170.F.1.1	5732	0.40	1848	18,814	10.5	2.848	9.12	0.11377	0.88	1860	16	−5
170.A.2.1	2470	0.00	3034	36,902	12.6	2.882	1.34	0.11360	0.51	1858	9	−4
170.G.1.1	1047	0.20	1670	57,535	35.6	3.057	2.21	0.11360	0.77	1858	14	+2
170.E.3.2	11,733	0.01	2541	54,550	22.2	3.098	5.80	0.11349	0.64	1856	12	+3
170.F.2.1	12,083	0.00	1084	40,918	39.0	3.076	1.10	0.11341	1.37	1855	25	+2
170.C.2.1	24,144	0.00	283	24,038	87.8	2.934	1.83	0.11331	1.73	1853	31	−2
170.F.1.8	3291	0.12	1657	39,834	24.8	3.104	1.74	0.11309	0.75	1850	14	+3
170.B.1.2	9389	0.23	1780	55,107	32.0	2.965	1.07	0.11308	0.81	1849	15	−2
170.A.2.2	921	0.25	1827	50,186	28.4	3.063	1.00	0.11308	0.81	1849	15	+2
170.G.2.4	2674	0.15	2333	61,028	27.0	2.985	1.01	0.11296	0.65	1848	12	−1
170.E.1.1	15,988	0.14	2303	56,382	25.3	2.930	1.90	0.11295	0.66	1847	12	−3
170.B.1.1	1089	0.24	1708	70,472	42.6	2.958	2.83	0.11295	1.23	1847	22	−2
170.D.1.1	2966	0.41	1479	77,690	54.3	2.917	1.13	0.11281	1.20	1845	22	−3
170.E.2.1	8958	0.39	1071	46,612	45.0	3.081	1.96	0.11169	1.10	1827	20	+1
170.B.1.3	13,769	0.34	927	51,447	57.3	3.119	1.17	0.11102	1.14	1816	21	+1
170.G.1.3	1042	0.41	1634	62,454	39.5	3.058	1.95	0.11087	1.13	1814	21	−1
Not considered: >10% discordance (n = 8)												
170.D.1.3	23,508	0.00	303	52,087	177.3	3.358	1.92	0.11530	1.84	1885	33	+12
170.D.2.2	16,474	0.74	231	50,605	226.8	2.996	3.51	0.09522	14	1532	259	−24
170.F.1.4	3109	0.22	2106	29,027	14.2	2.712	1.02	0.11195	0.74	1831	13	−12
170.F.1.5	1574	0.43	1553	18,671	12.4	2.768	9.05	0.10979	1.13	1796	20	−12
170.F.1.7	9050	0.00	2314	28,796	12.9	3.310	9.79	0.11490	0.64	1878	11	+11
170.G.1.2	12,184	0.42	916	116,569	131.5	3.571	18.25	0.11190	11	1830	190	+15
170.G.2.1	7773	0.54	636	42,205	68.5	4.171	21.74	0.12016	17	1959	303	+32
170.G.2.3	20,656	0.28	283	56,548	206.6	3.314	2.10	0.11710	1.96	1912	35	+13
Not considered: >1% common Pb (n = 2)												
170.G.2.2	21,848	1.38	222	60,782	283.3	3.242	1.99	0.10053	3.42	1634	64	−7
170.D.1.2	28,346	1.28	145	63,550	453.0	3.093	2.52	0.10438	4.16	1703	77	−7
Not considered: Instrument instability (n = 3)												
170.A.1.1	15,472	0.48	578	61,477	110.0	3.251	1.69	0.10899	1.59	1783	29	+3
170.E.1.2	9820	0.16	1854	37,713	21.0	3.097	1.70	0.11290	0.77	1847	14	+3
170.E.3.3	2874	0.00	1052	45,153	44.4	3.022	5.96	0.11521	0.92	1883	17	+2
East Tennant (ET2786115) - GA sample no. **2786115**; drill hole DDH 005 (depth 168.89 m–169.04 m), lat −19.5201, long 135.9558 (GDA94)												
1844 ± 3 Ma population (n = 15)												
115.F.1.1	17,089	0.15	5531	43,921	8.2	2.937	0.80	0.11335	0.44	1854	8	−2
115.G.4.1	14,744	0.10	2990	41,194	14.2	3.287	1.05	0.11317	0.49	1851	9	+9
115.G.1.1	16,354	0.07	3235	30,310	9.7	2.894	1.24	0.11311	0.90	1850	16	−4
115.D.3.1	18,217	0.02	8191	52,096	6.6	3.061	1.13	0.11311	0.23	1850	4	+2
115.E.1.1	15,234	0.02	5446	38,712	7.3	3.239	1.22	0.11308	0.27	1850	5	+7
115.B.2.1	16,084	0.07	5899	63,277	11.1	2.827	1.40	0.11294	0.25	1847	5	−7
115.D.2.1	19,077	0.03	9780	59,196	6.3	2.901	1.17	0.11286	0.22	1846	4	−4
115.A.2.1	18,799	0.04	9001	60,196	6.9	2.973	1.25	0.11286	0.23	1846	4	−1
115.F.1.2	14,566	0.03	4504	38,065	8.7	2.826	1.68	0.11262	0.27	1842	5	−7
115.C.1.1	17,501	0.04	7202	48,614	7.0	2.860	1.07	0.11254	0.24	1841	4	−6
115.C.2.1	16,485	0.02	5736	44,790	8.1	2.846	0.80	0.11254	0.24	1841	4	−6
115.A.1.1	17,375	0.06	6187	55,623	9.3	2.905	0.81	0.11252	0.29	1841	5	−4
115.B.5.1	15,682	0.09	4306	30,929	7.4	3.020	2.60	0.11245	0.33	1839	6	−0
115.D.1.1	15,562	0.05	3401	39,930	12.1	3.068	0.86	0.11229	0.38	1837	7	+1
115.G.3.1	16,144	0.08	5125	49,071	9.9	3.239	1.42	0.11209	0.35	1834	6	+6
Not considered: Misplaced beam (n = 3)												
115.A.3.1	13,447	0.24	3151	23,285	7.6	3.422	3.74	0.10949	2.86	1791	52	+9
115.B.1.1	14,085	0.01	4455	37,773	8.8	2.941	1.30	0.11288	0.32	1846	6	−3
115.G.2.1	18,240	0.06	7851	61,705	8.1	2.829	2.02	0.11271	0.29	1844	5	−7
Not considered: Instrument instability (n = 2)												
115.B.3.1	15,060	0.08	7584	48,616	6.6	3.017	0.78	0.11241	1.72	1839	31	−0
115.E.2.1	14,974	0.06	5017	49,853	10.3	3.131	2.27	0.11319	1.14	1851	21	+4

(*continued on next page*)

Table 1 (*continued*)

SampleNo.plug. grain.spot	Y (ppm)	206Pbc (%)	U (ppm)	Th (ppm)	232Th /238U	238U /206Pb	±1σ (%)	207Pb /206Pb	±1σ (%)	207Pb/206Pb Date (Ma)	±1σ (Ma)	Disc. (%)
Murphy Inlier (MI2786177) - GA sample no. **2786177**; outcrop, lat −17.8946, long 137.7205 (GDA94)												
1845 ± 4 Ma population (n = 13)												
177.D.1.1	16,218	0.00	4767	48,067	10.4	3.127	1.58	0.11351	0.35	1856	6	+4
177.E.2.1	15,803	0.00	4138	50,241	12.5	3.146	1.75	0.11310	0.36	1850	6	+4
177.E.2.2	17,672	0.00	5171	54,351	10.9	3.079	1.20	0.11305	0.35	1849	6	+2
177.B.3.1	20,431	0.00	5693	39,251	7.1	3.052	1.10	0.11304	0.31	1849	6	+1
177.B.1.1	14,425	0.05	3463	39,594	11.8	3.127	0.85	0.11294	0.40	1847	7	+4
177.A.2.1	22,267	0.00	6038	44,007	7.5	3.058	0.96	0.11290	0.30	1847	5	+1
177.B.2.1	16,491	0.00	3435	39,202	11.8	3.039	1.98	0.11276	0.38	1844	7	+1
177.B.1.2	21,043	0.00	5083	48,193	9.8	3.048	1.73	0.11276	0.34	1844	6	+1
177.E.1.1	19,601	0.01	4556	45,454	10.3	3.009	1.05	0.11270	0.34	1843	6	−0
177.D.3.1	19,073	0.05	4091	42,534	10.7	3.148	1.45	0.11269	0.62	1843	11	+4
177.E.3.1	21,267	0.02	4993	47,305	9.8	3.139	1.53	0.11240	0.57	1839	10	+3
177.E.3.2	22,118	0.00	5722	47,857	8.6	3.100	1.45	0.11218	0.34	1835	6	+2
177.B.4.1	25,026	0.05	5106	47,362	9.6	3.037	1.17	0.11207	0.34	1833	6	−0
Not considered: >10% discordance (n = 3)												
177.C.2.1	17,766	0.04	4803	39,749	8.5	3.803	19.47	0.11566	11	1890	204	+23
177.A.2.2	3096	1.25	3029	25,432	8.7	5.560	16.57	0.11725	4.69	1915	84	+48
177.C.1.1	26,379	0.00	6499	45,367	7.2	2.452	12.84	0.09914	12	1608	219	−44
Not considered: Instrument instability (n = 3)												
177.C.3.1	18,179	0.01	4783	31,496	6.8	3.449	22.93	0.10562	27	1725	494	+5
177.D.2.1	16,806	0.01	3779	41,709	11.4	3.235	2.36	0.11209	0.81	1834	15	+6
177.A.1.1	21,769	0.03	5095	45,437	9.2	3.043	3.14	0.10790	3.45	1764	63	−4

paucity of cordierite in the sample best correspond to field 6, and suggest that peak conditions were 2.8–3.3 kbar and 655–680 °C (Fig. 7A). Although this is a relatively narrow field in *P–T* space, the proportion of sillimanite to cordierite changes significantly across fields 6 and 8, suggesting that the rock was unlikely to have experienced pressures and temperatures far inside field 8, as this would have led to the formation of abundant cordierite at the expense of sillimanite (Fig. 7B and C). The absence of ilmenite in the sample supports the interpreted peak conditions, but does not provide a robust constraint because it is very sensitive to oxidation state, and is only predicted to occur in trace amounts at near-peak pressures and temperatures (Fig. 7C). The peak conditions correspond to a high apparent thermal gradient in excess of 190 °C/kbar.

6. Discussion

6.1. Interpretation of petrographical, geochronological and thermodynamic data

6.1.1. Sample TC2765170 (Tennant Region)

We interpret the pervasive foliation in sample TC2765170 to reflect an episode of *syn*-tectonic metamorphism in the Tennant Region. An absence of quantitative thermobarometric data or key mineral phases for this sample preclude a precise estimate of peak metamorphic conditions. Nevertheless, the absence of chlorite, abundance of garnet and biotite, and appearance of chessboard extinction in quartz grains (e.g. Stipp et al., 2002) imply that peak metamorphic conditions were within the amphibolite facies. As monazite and garnet are included within the pervasive foliation, but are not wrapped by it (Fig. 5A), we infer that both minerals grew during this tectono-metamorphic event. This is also supported by the highly variable Y concentration in monazite from this sample, which likely reflects variations in garnet stability during monazite growth (e.g. Kelly et al., 2015). Thus, sample TC2765170 is interpreted to record amphibolite-facies metamorphism and deformation at 1858 ± 7 Ma. The more discrete shear bands in the sample, which overprint the early assemblage (Fig. 4A), are interpreted to reflect a second episode of deformation at a relatively low metamorphic grade, given the minor recrystallisation of mica and magnetite associated with this younger fabric.

6.1.2. Sample ET2786115 (East Tennant area)

As the peak metamorphic assemblage in the sample from the East Tennant area also defines a tectonic fabric, we interpret that metamorphism was coeval with deformation. Phase equilibria modelling suggests that peak metamorphic conditions in this sample were 2.8–3.3 kbar and 655–680 °C, which corresponds to extremely high apparent thermal gradients of > 190 °C/kbar. Syn-tectonic metamorphism is also consistent with amoeboid grain boundaries and chessboard extinction in quartz grains observed in this sample (e.g. Stipp et al., 2002). Several observations indicate that monazite most likely grew at around the timing of peak metamorphism. First, monazite is not included in andalusite, which is interpreted as prograde. Second, monazite is mostly associated with biotite and sillimanite, which form part of the peak metamorphic assemblage in this sample and define the main tectonic fabric. Third, there is no evidence that biotite or sillimanite have been significantly affected by retrograde metamorphism or alteration. Thus, we interpret that the 1844 ± 3 age of monazite from sample ET2786115 also dates the deformation and metamorphism in this sample.

6.1.3. Sample MI2786177 (Murphy Inlier)

The moderately developed metamorphic fabric in the Murphy Inlier sample, which is well-developed and steeply dipping at outcrop scale, is also interpreted to reflect metamorphism accompanied by deformation. The lack of key index minerals present in this sample preclude a precise estimate of metamorphic conditions. Nevertheless, the abundance of relatively coarse-grained biotite and muscovite and the absence of chlorite suggest that conditions were within the amphibolite facies. As monazite is associated with this metamorphic assemblage and a tectonic foliation, and as the sample contains no evidence of a younger or older event in which monazite is likely to have grown, we interpret that metamorphism and deformation occurred during monazite growth at 1845 ± 4 Ma.

6.2. Refining the 1860–1840 Ma tectono-metamorphic and magmatic evolution of the Tennant Region, East Tennant area, and the Murphy Inlier

New geochronological data (this study) and recent U-Pb age data (Cross et al., 2020; Farias et al., 2021; Huston et al., 2020; Kositcin and Carson, 2019; Kositcin et al., 2020) permit a revised model for the tectono-magmatic evolution of the region encompassed by the East Tennant area, Tennant Region and the Murphy Inlier. This is presented in Fig. 8 and discussed below.

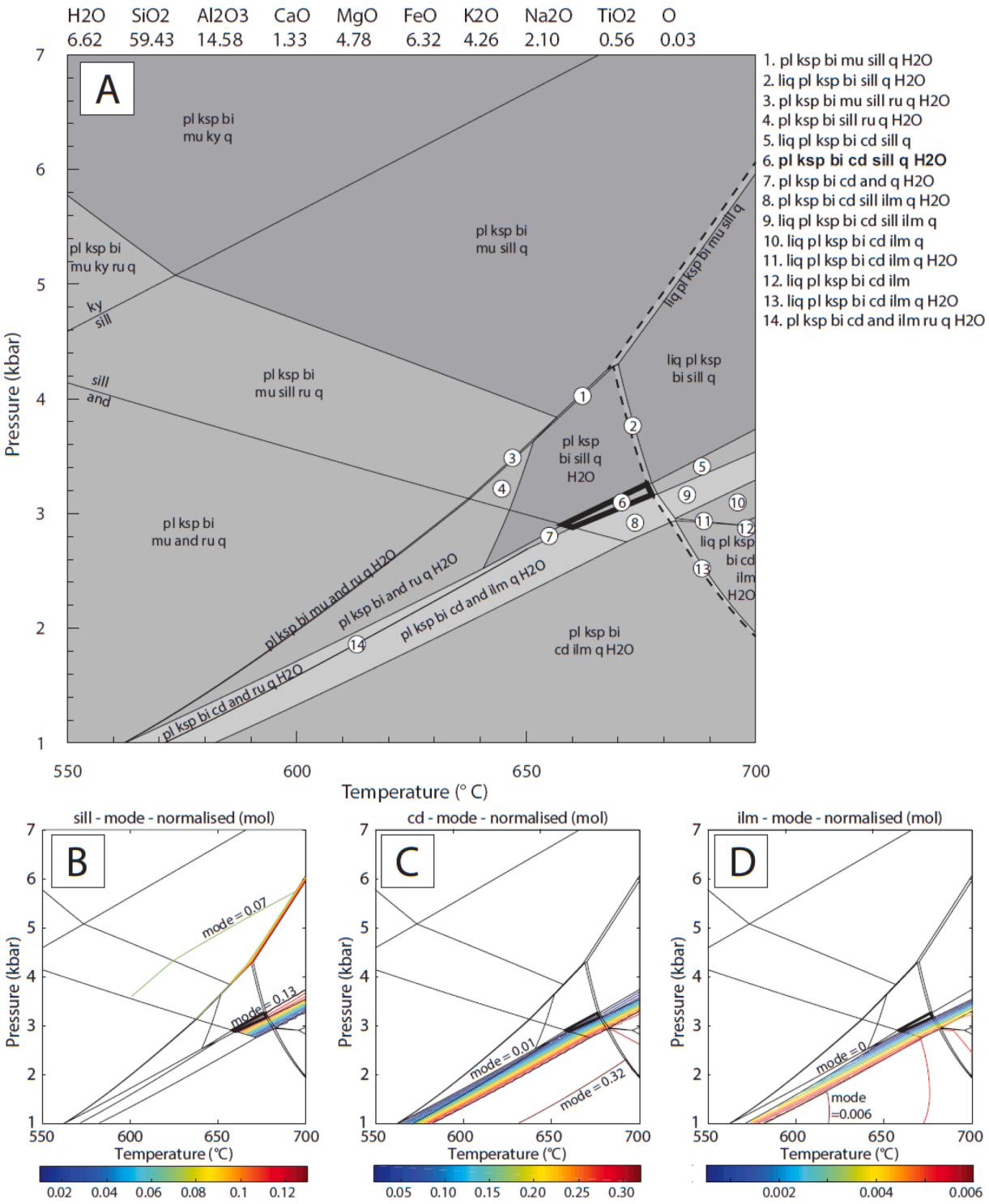

Fig. 7. (A) Calculated P–T pseudosection for sample ET2786115 from the East Tennant area. The bulk composition in mol% is given above the pseudosection. The interpreted peak field (field 6) is outlined in bold, whereas the solidus is shown as a dashed line. (B through D) The same pseudosection as in (A) with coloured contours for the modal proportion (in mol%) of sillimanite, cordierite, and ilmenite, respectively. Abbreviations: albite (ab), andalusite (and), biotite (bi), cordierite (cd), ilmenite (ilm), K-feldspar (ksp), kyanite (ky), muscovite (mu), plagioclase (pl), quartz (q), rutile (ru), silicate melt (liq), sillimanite (sill).

6.2.1. 1860–1855 Ma: Crustal shortening (D_1/M_1) in the Tennant Region

Our 1858 ± 7 Ma age for deformation and metamorphism of supracrustal rocks in the Tennant Region represents the first direct age of a regional foliation formed during the Tennant Event (Donnellan, 2013). This age, when combined with existing data, helps to clarify the chronology and deformation episodes encompassed in this event (Fig. 8). Previously documented crystallisation and maximum deposition ages from felsic volcanic rocks of the Warramunga Formation and Junalki Formation constrain their deposition to around 1860 Ma (Compston, 1995; Maidment et al., 2006; Maidment et al., 2013; Smith, 2001). Upright folding of these units along broadly east-trending axes occurred prior to ~ 1855 Ma, as they are unconformably overlain by 1855–1845 Ma strata of the Yungkulungu Formation and equivalent units (Blake, 1984; Donnellan, 2013). Intrusive rocks of the 1855–1845

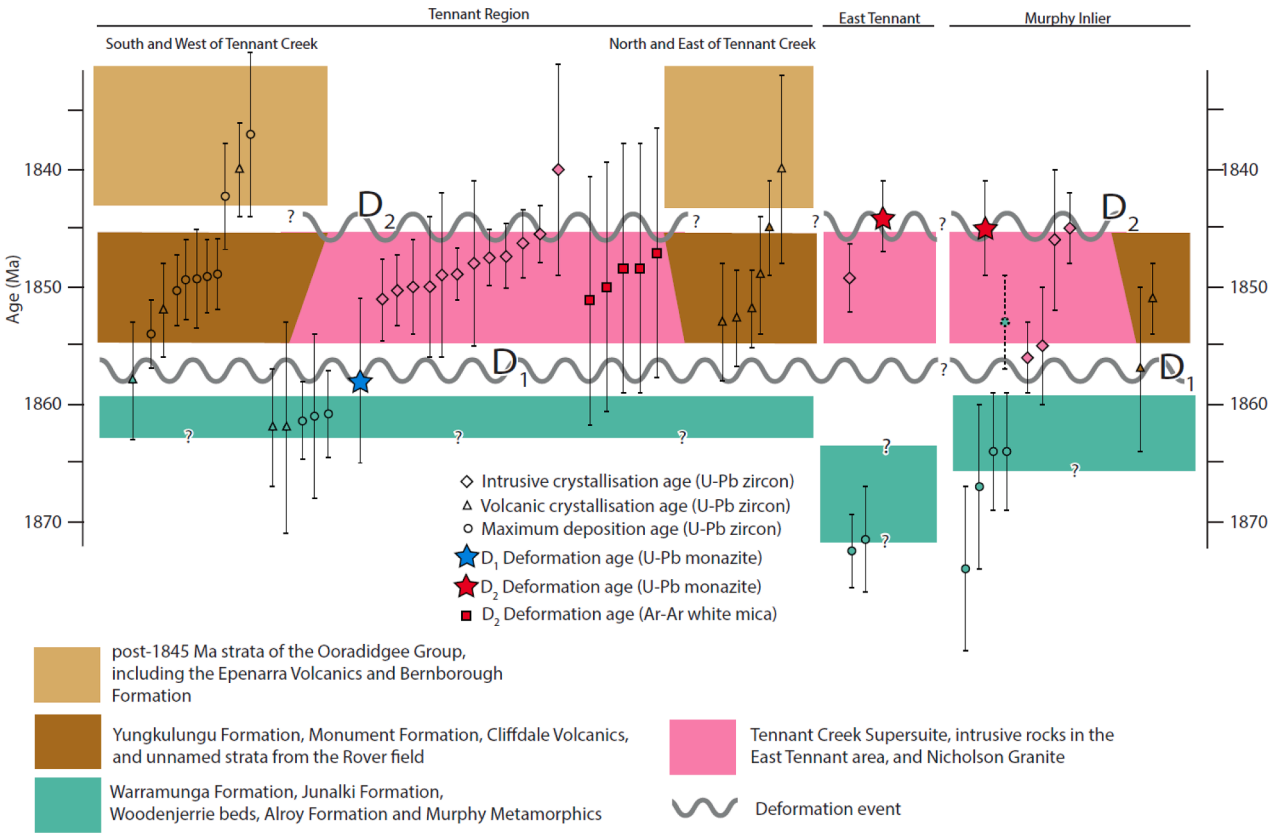

Fig. 8. 1870–1830 Ma Tectono-stratigraphic framework for the Warramunga and Murphy Provinces. Note that deformation ages do not correspond to any stratigraphy, i.e. the $^{40}Ar/^{39}Ar$ ages were not collected from the Tennant Creek Supersuite. Age data from this study, Huston et al. (2020), Cross et al. (2020), Farias et al. (2021), Maidment et al. (2013), Smith (2001), Compston (1995), Compston and McDougall (1994), Fraser et al. (2008), Claoué-Long et al. (2008), Kositcin et al. (2013), Kositcin et al. (2014), Page et al. (2000), Kositcin and Carson (2019) and Kositcin et al. (2020). Ages with errors>10 million years are omitted. A single age (Hollis et al., 2010) is dashed and not discussed on the basis that it is a statistical outlier.

Ma Tennant Creek Supersuite locally cross-cut these folds and their associated cleavage in ~ 1860 Ma stratigraphy, and contain xenoliths of Warramunga Formation that preserve a tectonic cleavage (Donnellan, 2013; Donnellan et al., 1995; Huston and Cozens, 1994; Nguyen et al., 1989). In conjunction with our new 1858 ± 7 Ma age, these results establish a regional deformation event in the Tennant Region at 1860–1855 Ma, which we term D_1 (Fig. 8). In outcropping stratigraphy D_1 is mostly associated with low-grade metamorphism (M_1) and, based on the east–west orientation of D_1 fold axes, has been interpreted to reflect north–south compression (Donnellan, 2013; Rattenbury, 1994). The significance of this compressional episode is also marked by a significant change in depositional environment, from the turbiditic setting of the ca.1860 Ma Warramunga Formation to the shallow-marine and subaerial setting of siliciclastic and volcanic rocks of the ca. 1855–1810 Ma Ooradidgee Group, including the Yungkulungu Formation (Donnellan et al., 1995).

Our data indicate that D_1/M_1 was not exclusively a low-grade event, as the amphibolite-facies rocks of uncertain stratigraphic affiliation west-southwest of Tennant Creek (Crohn and Oldershaw, 1965), from which sample TC2765170 was obtained, underwent metamorphism (M_1) during this event. Our 1858 ± 7 Ma metamorphic age from this sample precludes interpretations of this package as part of the Ooradidgee Group (e.g. Donnellan and Johnstone, 2004) and instead indicates that these rocks may be age-equivalents to the Warramunga Formation. We interpret the ca. 1827 Ma age from a felsic rock in this package to be a magmatic age of a younger felsic intrusive unit (Compston, 1995). Our results indicate that supracrustal rocks in this region pre-date mineralisation at Tennant Creek, and are thus potentially prospective for mineralisation (Donnellan, 2013). Although the lithology of this package is broadly consistent with it being a more metamorphosed part of the Warramunga Formation, it is also possible that these rocks pre-date the Warramunga Formation (e.g. Crohn and Oldershaw, 1965), and therefore could represent a part of the stratigraphy so far not recognised in the area. There is no detrital zircon data available for this package.

The geochronological data and overprinting relationships presented above indicate that the Warramunga Formation was deposited at ~ 1860 Ma and regionally deformed and metamorphosed during D_1/M_1 between 1860 and 1855 Ma (Fig. 8). This is difficult to reconcile with Maidment et al. (2013) and McPhie (1993), who interpreted peperitic margins on some high-level felsic intrusions of the Tennant Creek Supersuite emplaced at ~ 1847 Ma to indicate that the Warramunga Formation remained unconsolidated at that time. It is possible that a re-examination of the peperitic textures, and the rocks into which they intrude, is warranted. We note in this context that the margins of many of these high-level intrusive rocks have been deformed (Donnellan et al., 1995), which may render interpretations of their primary emplacement textures suspect. Another possibility is that the intruded sediments belong to the Yungkulungu Formation, or equivalent coeval units, rather than the older Warramunga Formation.

6.2.2. 1860–1855 Ma: Evidence for D_1/M_1 in the Murphy Inlier and East Tennant area

Recently published ages from the Nicholson Granite and Murphy Metamorphics reinforce existing age data and field relationships that indicate that the Murphy Inlier underwent crustal shortening, characterised by east-trending upright folds and greenschist-facies metamorphism, between 1860 and 1855 Ma, as shown in Fig. 8 (Hanley,

1996; Kositcin et al., 2020; Kositcin et al., 2013; Kositcin and Carson, 2019; Page et al., 2000). We term this deformation and metamorphism D_1 and M_1, respectively, of the Murphy Event (Ahmad et al., 2013). Thus, the timing, style and broad trend of regional deformation and metamorphism during D_1/M_1 in the Murphy Inlier is remarkably similar to that in the Tennant Region (e.g. Ahmad and Scrimgeour, 2013).

Several observations suggest that D_1/M_1 also affected the East Tennant area at 1860–1855 Ma. First, D_1/M_1 in the Tennant Region and Murphy Inlier were extensive, resulting in upright folding along>100 km of strike length in each region and the development of a regional tectonic fabric (Ahmad et al., 2013; Donnellan 2013). Second, D_1 folds in the Tennant Region trend east and the magnetic character of these structures can be traced eastwards into the East Tennant area, with no evidence of a structural break (e.g. Clark et al., 2021b). Third, despite the challenges of seeing through the ca. 1845 Ma tectono-metamorphism in the East Tennant area characterised by sample ET2786115 (see below), evidence of an earlier lower-grade, but more widespread, event may be recorded north of the Gulunguru Fault (Fig. 2). In this area, upright folds in sub-greenschist facies rocks of the Alroy Formation are well preserved, trend east- to northeast, and are associated with a well-developed axial-planar cleavage (Clark et al., 2021a). We interpret these structures as evidence that the East Tennant area may have experienced the same early episode of regional crustal shortening (D_1) as the Tennant Region and the Murphy Inlier. Finally, given that 1855–1845 Ma magmatism in the Tennant Region and the Murphy Inlier were immediately preceded by, and therefore likely associated with, D_1 crustal shortening (see below) it seems reasonable to conclude that an episode of deformation (D_1) also immediately preceded coeval magmatism in the East Tennant area. The above information, taken together, indicates that the East Tennant area most likely experienced an episode of crustal shortening (D_1) between 1860 and 1855 Ma (Fig. 8).

6.2.3. 1855–1845 Ma: Igneous activity in the central part of the NAC

The emplacement and coeval eruption of the Nicholson Granite and Cliffdale Volcanics at 1855–1845, following regional deformation (D_1) in the Murphy Inlier, is well documented (Ahmad et al., 2013; Page et al., 2000; Kositcin et al., 2020). Recent geochronological data and interpretation of potential-field geophysical data indicates that the East Tennant area was also affected by significant ~ 1850 Ma igneous activity (Clark et al., 2021b; Cross et al., 2020). In regards to the Tennant Region, geochronological and geochemical data indicate that the lowermost package of the Ooradidgee Group is cogenetic with the Tennant Creek Supersuite (e.g. Donnellan, 2013). This package includes the Yungkulungu Formation and the Monument Formation, and unassigned coeval strata in the eastern part of the Tennant Region and the Rover field (e.g. Cross et al., 2020; Farias et al., 2021; Donnellan, 2013). As strata of this combined 1855–1845 Ma volcano-plutonic episode unconformably overlie or cross-cut D_1 folds (Blake, 1984; Donnellan, 2013; Nguyen et al., 1989), we argue that the Tennant Creek Supersuite must largely post-date regional folding during the Tennant Event (Fig. 8), in contrast to existing models for the evolution of the Tennant Region shown in Fig. 3 (Donnellan, 2013; Maidment et al., 2013; Skirrow et al., 2019).

6.2.4. 1845–1840 Ma: Discrete shearing and localised metamorphism (D_2/M_2)

Previous studies (e.g. Ahmad and Wygralak, 1989; Gardner, 1978) have interpreted all ductile deformation and metamorphism in the Murphy Province to pre-date eruption of the Cliffdale Volcanics and emplacement of the Nicholson Granite at 1855–1845 Ma. However, our 1845 ± 4 Ma age for the formation of an amphibolite-faces foliation in sample MI2786177 implies that an east-trending fabric developed in the Murphy Metamorphics during the waning stage of, or after, 1855–1845 Ma igneous activity. As there is robust evidence that regional folding (D_1 of the Murphy Event) occurred at 1860–1855 Ma (e.g. Ahmad and Wygralak, 1989; Kositcin et al., 2013; Kositcin and Carson, 2019; Page et al., 2000), we suggest that a second episode of deformation and metamorphism (D_2/M_2 of the Murphy Event) affected the Murphy Province at ~ 1845 Ma (Fig. 8). Thermal affects due to the emplacement of the Nicholson Granite are likely to have contributed to the metamorphism in sample MI2786177, which was collected only one kilometre from one of the granite intrusions. Nevertheless, the amphibolite-facies fabric in sample MI2786177, which is penetrative in outcrop, indicates that significant deformation occurred in the Murphy Inlier at 1845 ± 4 Ma. Given the apparent absence of a tectonic fabric within the cores of Nicholson Granite bodies or in the Cliffdale Volcanics (Gardner, 1978), we interpret that D_2 strain was partitioned into discrete shear zones, mostly within the already tightly-folded Murphy Metamorphics. This hypothesis is consistent with Ahmad and Wygralak's (1989) documentation of mica-rich shear zones in the Murphy Inlier that cross-cut D_1 folding in the region, but are otherwise not chronologically constrained. Although our interpretation that D_2 deformation in the Murphy Inlier post-dates the relatively flat-lying Cliffdale Volcanics appears contradictory at first glance, outcrop of the volcanics is mostly concentrated around 25 km to the northeast, away from the main outcrops of the Murphy Metamorphics that were the focus of D_2 strain. Thus, the lack of documented D_2 shear zones in the Cliffdale Volcanics cannot be used to infer timing relationships in this case. We note that the constraints on the timing of deformation are complex, and that more work is likely to improve our understanding of the tectono-metamorphic evolution of the Murphy Inlier.

Our new monazite ages reveal that the East Tennant area also records the development of a ductile deformation fabric during amphibolite-facies metamorphism at 1844 ± 3 Ma. The lack of basement exposure in the East Tennant area precludes constraining the structural context of this deformation and metamorphism at outcrop scale. However, given that the East Tennant area likely experienced an episode of crustal shortening at 1860–1855 Ma (D_1), we propose that sample ET2786115 records a second episode of deformation and metamorphism (D_2/M_2) at 1844 ± 3 Ma. Potential field data reveal that sample ET2786115 was collected in close proximity to a major northeast-trending shear zone, the Gulunguru Fault (Fig. 2). This may indicate that D_2 in the East Tennant area was associated with significant strain partitioning within an already tightly folded package, resulting in spatially restricted deformation and metamorphism, similar to D_2/M_2 in the Murphy Province. This event framework is also supported by the potential-field data interpretation of the East Tennant area as a whole, which reveals the existence of several major east- to northeast-trending (D_2) shear zones that show a late-syn to post timing relationship with the plutons of the Tennant Creek Supersuite (Clark et al., 2021b).

The same overprinting relationship can be observed in the Tennant Region, where most studies recognise steeply-dipping shear zones that trend east- to northeast and west- to northwest, and developed at a late stage during the 1860–1845 Ma Tennant Event (Hill et al., 2015; Donnellan, 2013; Donnellan, 1995; Nguyen et al., 1989; Crohn and Oldershaw, 1965; Skirrow and Walshe, 2002). This is consistent with our documentation of a shear fabric that cross-cuts the 1860–1855 Ma S_1 foliation in sample TC2765170 (Fig. 4A). A maximum age (ca. 1845 Ma) for these shear zones is provided by intrusive rocks of the 1855–1845 Ma Tennant Creek Supersuite, which are locally deformed by these structures (Donnellan, 2013; McPhie, 1993; Nguyen et al., 1989). A minimum age of ~ 1840 Ma is provided by younger uncertainty bounds on $^{40}Ar/^{39}Ar$ ages from muscovite associated with these structures, as shown in Fig. 8 (Fraser et al., 2008; Compston and McDougall, 1994; Nguyen et al., 1989; Donnellan, 2013). In the Tennant Region, the development of these shear zones has been included within D_1 as D_{1a} (Donnellan, 2013). However, given that these structures must have experienced movement between 1845 and 1840 Ma, we suggest that they represent a separate deformation event, D_2, within the broader Tennant Event. Several additional pieces of evidence support this interpretation. First, D_1 and D_2 are separated by a magmatic episode

lasting ~ 10 million years (Fig. 8) which included the deposition of volcanic units that unconformably overly D_1-affected strata (Donnellan, 2013). Second, D_1 and D_2 differ markedly in structural style, with the former characterised by regional folding and the latter by strong strain partitioning and the formation of major, discrete, steeply-dipping dextral shear zones (Skirrow and Walshe, 2002; Donnellan et al., 1995; Donnellan, 2013). Finally, a significant change in the orientation of the stress field between D_1 and D_2 is required to account for the change from upright, east-trending folds of D_1 to the steeply-dipping, dextral shear zones that developed during D_2 (Donnellan et al., 1995). Although we cannot completely rule out that deformation was continuous, in part, between D_1 and D_2 (e.g. Donnellan, 2013), we consider the separation of D_1 and D_2 into discrete events to better represent their significance within the stratigraphic and magmatic history of the region.

6.2.5. Connecting the dots: Widespread 1860–1840 Ma tectono-magmatism in the (present day) centre of the NAC

Similarities in timing, orientation, folding style and regional metamorphic grade indicate that the D_1/M_1 events in the Tennant Region and Murphy Inlier were part of the same regional event, which also affected the East Tennant area (Fig. 8). This episode was characterised by upright folding and mostly low-grade metamorphism at 1860–1855 Ma, signifying contractional deformation across a > 600 km long, east- to northeast-trending corridor stretching from the Tennant Region to the Murphy Inlier (Fig. 2). Given the overall east- to northeast trend of this corridor, we suggest that shortening during D_1 was in response to north-northwest–south-southeast compression across the present-day central part of the NAC.

Although the comparable timing of 1855–1845 Ma magmatism in the Warramunga and Murphy Provinces has been observed previously (e.g. Ahmad and Scrimgeour, 2013), there has been little attempt to link the expression of this magmatism in a geographic sense. However, recent interpretation of potential-field data (Clark et al., 2021b) and new age constraints from intrusive rocks (Cross et al., 2020) reveal that the East Tennant area was also affected by extensive plutonism at ~ 1850 Ma. We interpret these new results to represent a 'missing link' that reveals a broadly continuous belt of 1855–1845 Ma magmatism from the Tennant Region, including the Rover field, through the East Tennant area to the Murphy Inlier (Fig. 2 and Fig. 8).

The Murphy Inlier, East Tennant area, and the Tennant Region all underwent a subsequent episode of deformation (D_2), characterised by strain partitioning and the development of regional shear zones, at ca. 1845–1840 Ma (Fig. 8). It is possible to map the expression of D_2 between the East Tennant area and the Tennant Region. For example, the Gulunguru Fault in the East Tennant area can be traced west into the Tennant Region (see Fig. 2), where it connects with ~ 1845 Ma (D_2) structures (e.g. Hill et al., 2015). Structural links between the East Tennant area and the Murphy Inlier are less conclusive, as the Murphy Inlier is located north of the main northeast trend of structures in the East Tennant area (Fig. 2), and the transition is masked by thick basin cover (Fig. 2). However, as shown in Fig. 2, the Murphy Metamorphics also crop out in the Carrara Range Inlier (Rawlings et al., 2008), which does lie along the northeast projected trend of the Gulunguru Fault. Here, the Murphy Metamorphics contain an east- to northeast trending foliation (Rawlings et al., 2008), which is consistent with this inlier also recording D_2 deformation.

D_2/M_2 marks a significant change in tectono-metamorphic style from regional upright folding and mostly low-grade metamorphism that characterise D_1/M_1 to strong strain partitioning into discrete shear zones (e.g. Clark et al., 2021b) and the formation of amphibolite-facies assemblages in the East Tennant area and the Murphy Inlier. These changes reflect a different stress field orientation (e.g. Donnellan et al., 1995), possibly accompanying an evolution in the rheological architecture from layer-cake sediments into a tightly folded package that provided more steeply-dipping anisotropies. Widespread magmatism between M_1 and M_2 is likely to have contributed to the broad difference in metamorphic grade between these two events. However, it is important to note that M_2 assemblages, especially in East Tennant, are extensive (Clark et al., 2021a). Thus, we interpret M_2 metamorphism to be the product of a regionally elevated geotherm, largely due to, and outlasting, extensive 1855–1845 Ma magmatism, as opposed to localised contact metamorphism restricted to the immediate vicinity of intrusive bodies.

6.3. Implications for the 1860–1840 Ma tectonic setting of the NAC

A comprehensive discussion of the tectonic setting of the Tennant Region, East Tennant area and the Murphy Inlier at 1860–1840 Ma would require a detailed account of geochemical data, amongst others, and is beyond the scope of this study. Nevertheless, our results provide important new constraints for existing tectonic models. For the Tennant Region, Maidment et al. (2013) and Donnellan et al. (1995) favour a tectonic model involving continuous extension and/or the presence of a mantle hot spot as the driver for the deposition of the Warramunga Formation and subsequent Tennant Creek Supersuite magmatism. However, we demonstrate that this magmatism started in the waning stages of an episode of crustal shortening (D_1) and regional metamorphism (M_1). We suggest that crustal shortening was an important precursor to 1855–1845 Ma magmatism, but that magmatism was likely a response to a period of extension that also facilitated accommodation of volcanosedimentary strata in the Tennant Region and Murphy Inlier (e.g. Donnellan et al., 1995; Maidment et al., 2013). The footprint of D_1 and subsequent magmatism, which forms a domain over 600 km in length, indicates that much of the present-day central part of the NAC underwent significant tectonism, from ~ 1870–1860 Ma extension (?) and the deposition of a widespread turbiditic package (e.g. Maidment et al., 2020), into north–south compression between 1860 and 1855 Ma, resulting in basin inversion. Extensive 1855–1845 Ma magmatism, potentially induced by a period of extension, was followed by renewed, or continued, contraction and deformation along a system of steeply-dipping regional shear zones between 1845 and 1840 Ma.

Our identification of a continuous 1860–1840 Ma tectono-magmatic domain in the centre of the NAC has implications for the understanding of the tectonic evolution of the NAC as well as global paleo-tectonic reconstructions. For example, Betts et al. (2015) present a reconstruction of the NAC that features convergent-margin magmatism at ~ 1860 Ma in the Aileron Province and ~ 1850 Ma in the Mount Isa Inlier, and Payne et al. (2009) present a model whereby northwest Laurentia collided with the NAC along a northwest-trending margin east of the Murphy Inlier at ca. 1870–1845 Ma. Both of these models feature convergent margins at a high angle to the present-day tectonic grain of the east-northeast trending, tectono-magmatic domain that connected the Tennant Region with the Murphy Inlier at 1860–1840 Ma. The significant deformation, metamorphism and magmatism that characterise this domain suggest that models that depict the locus of deformation and magmatism at this time to be focused solely around the present day margins of the NAC are too simplistic (e.g. Betts et al., 2015; Fraser et al., 2007; Zhao et al., 2004).

Potential field geophysical data suggest that the 1860–1840 Ma domain may extend northeast into the undercover continuation of the Mount Isa inlier (Fig. 1), although any connection with coeval tectono-metamorphism in this inlier (e.g. McDonald et al., 1997; Neumann et al., 2009) is masked by the intense reworking of the younger Isan Orogeny. To the west of the Tennant Region, the 1860–1840 Ma domain has been affected by younger deformation related to activity on the NAC's ancient southern margin (Scrimgeour, 2013). Nevertheless, the overall trend of the 1860–1840 Ma domain continues west-northwest, projecting towards the northernmost Lamboo Province and Pine Creek Orogen, which also record deformation and magmatism of this age (e.g. Ahmad and Hollis, 2013; Sheppard et al., 1999). Thus, the tectono-magmatic domain encompassing the Tennant Region and the Murphy Province may extend across a broader area of the NAC. We speculate that this

1860–1840 Ma tectonism may mark a transition in the locus of tectono-magmatic activity in the NAC, from the far north in the Arnhem Province at ca. 1880 Ma (e.g. Maidment et al., 2020; Whelan et al., 2017) to the Aileron and Tanami provinces in the south by ca. 1830 Ma (e.g. Scrimgeour, 2013).

7. Conclusions

New in-situ monazite ages from the East Tennant area, the Tennant Region, and the Murphy Inlier help constrain the tectono-metamorphic evolution and architecture of the central region of the NAC between 1860 and 1840 Ma, and support a new event framework that integrates sedimentation, deformation and metamorphism, and magmatism. Following the widespread deposition of 1870–1860 Ma turbiditic sediments (e.g. Cross et al., 2020; Donnellan, 2013; Ahmad et al., 2013), an episode of north–south crustal shortening (D_1) occurred at 1860–1855 Ma. This deformation resulted in the formation of upright folds and regional, mostly low-grade metamorphism (M_1) at the current level of exposure. D_1 preceded widespread felsic magmatism from 1855 to 1845 Ma, possibly driven by an episode of extension (Compston, 1995; Kositcin et al., 2013; Maidment et al., 2013; Page et al., 2000). A subsequent episode of deformation (D_2) is characterised by the development of major shear zones between 1845 and 1840 Ma. In the Tennant Region, D_2 is not associated with significant medium-grade metamorphism, whereas in the East Tennant area and the Murphy Inlier, D_2 is associated with low-pressure, amphibolite-facies assemblages (M_2). This most likely reflects an elevated geothermal gradient due to preceding, or partly coeval, magmatism. Taken together, these observations resolve 1860–1840 Ma tectono-magmatism in the central region of the NAC into discrete episodes that define a previously unrecognised continuous domain stretching over 600 km from the Tennant Region to the Murphy Inlier via the East Tennant area. We speculate that this domain marks an intermediate step in the 1880–1830 Ma migration of the locus of tectono-metamorphism in the NAC from north in the Arnhem Province to the south in the Aileron and Tanami provinces.

CRediT authorship contribution statement

A.D. Clark: Conceptualization, Methodology, Investigation, Writing – original draft, Visualization, Project administration. **L.J. Morrissey:** Methodology, Software, Formal analysis, Investigation, Writing – review & editing, Visualization. **M.P. Doublier:** Conceptualization, Writing – review & editing, Supervision. **N. Kositcin:** Software, Formal analysis, Investigation. **A. Schofield:** Conceptualization, Supervision. **R.G. Skirrow:** Data curation, Writing – review & editing.

Declaration of Competing Interest

The authors declare that they have no known competing financial interests or personal relationships that could have appeared to influence the work reported in this paper.

Acknowledgements

This study was carried out as part of Geoscience Australia's Exploring for the Future program and the MinEx CRC National Drilling Initiative. Laboratory staff at Geoscience Australia, in particular David DiBugnara, Chuck Magee, and Jo Tubby, are thanked for their meticulous preparation of sample material, SEM imaging, and set-up of the SHRIMP ion probe. We are grateful to David Huston and Simon Bodorkos for comments on an early version of the manuscript. Reviews by Fawna Korhonen and David Maidment are appreciated and significantly improved the manuscript. We also thank editors at PCR for their handling of the manuscript. Insights from discussions with Northern Territory Geological Survey staff, in particular Nigel Donnellan, are gratefully acknowledged. LJM is supported by an Australian Research Council DECRA Fellowship DE210101126. This paper is published with the permission of the CEO, Geoscience Australia.

Supplementary material

Supplementary data to this article can be found online at https://doi.org/10.1016/j.precamres.2022.106652.

References

Ahmad, M., Hollis, J.A., 2013. Chapter 5: Pine Creek Orogen. In: Ahmad, M., Munson, T. J. (Eds.), Geology and mineral resources of the Northern Territory, Northern Territory Geological Survey, Darwin. Special Publication 5, 5:1–5:133.

Ahmad, M., Munson, T.J., Wygralak, A.S., 2013. Chapter 8: Murphy Province. In: Ahmad, M., Munson, T.J. (Eds.), Geology and mineral resources of the Northern Territory, Northern Territory Geological Survey, Darwin. Special Publication 5, 8: 1–8:8.

Ahmad, M., Scrimgeour, I.R., 2013. Chapter 2: Geological Framework. In: Ahmad, M., Munson, T.J. (Eds.), Geology and mineral resources of the Northern Territory, Northern Territory Geological Survey, Darwin. Special Publication 5, 2:1–2:16.

Ahmad, M., Wygralak, A.S., 1989. Calvert Hills, Northern Territory, 1:250 000 Metallogenic Map Series explanatory notes, SE 53-8. Northern Territory Geological Survey, Darwin.

Ahmad, M., Wygralak, A.S., 2014. Calvert Hills, Northern Territory (Revised First Edition) 1:250 000 Geological Map Series, SE 53-8. Northern Territory Geological Survey, Darwin.

Aleinikoff, J.N., Schenk, W.S., Plank, M.O., Srogi, L., Fanning, C.M., Kamo, S.L., Bosbyshell, H., 2006. Deciphering igneous and metamorphic events in high-grade rocks of the Wilmington Complex, Delaware: Morphology, cathodoluminescence and backscattered electron zoning, and SHRIMP U-Pb geochronology of zircon and monazite. Geol. Soc. Am. Bull. 118, 39–64. https://doi.org/10.1130/B25659.1.

Bell, R.M., Hallof, P.G., 1962. Supplementary report on induced polarization survey BMR 3 & other areas near Tennant Creek, Northern Territory. CR1962-0001, https://geoscience.nt.gov.au/gemis/ntgsjspui/handle/1/59737.

Betts, P.G., Armit, R.J., Stewart, J., Aitken, A.R.A., Ailleres, L., Donchak, L., Hutton, L., Withnall, I., Giles, D., 2015. Australia and Nuna. In: Li, Z.X., Evans, D.A.D., Murphy, J.B. (Eds), Supercontinent Cycles Through Earth History. Geological Society, London, Special Publications, 424, 47-81. https://doi.org/10.1144/SP424.2.

Betts, P.G., Giles, D., Mark, G., Lister, G.S., Goleby, B.R., Ailleres, L., 2006. Synthesis of the Proterozoic evolution of the Mt Isa Inlier. Aust. J. Earth Sci. 53, 187–211. https://doi.org/10.1080/08120090500434625.

Blake, D.H., 1984. Stratigraphic correlations in the Tennant Creek region, central Australia: Warramunga Group, Tomkinson Creek beds, Hatches Creek Group, and Rising Sun Conglomerate. BMR J. Australian Geol. Geophys. 9, 41–47.

Blake, D.H., Tyler, I.M., Page, R.W., 2000. Regional Geology of the Halls Creek Orogen. In: Hoatson, D.M., Blake, D.H. (Eds), Geology and economic significance of the Palaeoproterozoic layered mafic-ultramafic intrusions in the East Kimberley, Western Australia, Australian Geological Survey Organisation, Bulletin 246, 35–62.

Carson, C.J., Worden, K.E., Scrimgeour, I.R., Stern, R.A., 2008. The Palaeoproterozoic evolution of the Litchfield Province, western Pine Creek Orogen, northern Australia: Insight from SHRIMP U-Pb zircon and in situ monazite geochronology. Precambr. Res. 166, 145–167. https://doi.org/10.1016/j.precamres.2006.12.016.

Cawood, P.A., Korsch, R.J., 2008. Assembling Australia: Proterozoic building of a continent. Precambr. Res. 166 (1–4), 1–35. https://doi.org/10.1016/j.precamres.2008.08.006.

Champion, D.C., 2013. Neodymium depleted mantle model age map of Australia: Explanatory notes and user guide. Record 2013/44. Geoscience Australia, Canberra. https://doi.org/10.11636/Record.2013.044.

Claoué-Long, J.C., Maidment, D., Donnellan, N., 2008. Stratigraphic timing constraints in the Davenport Province, central Australia: A basis for Palaeoproterozoic correlations. Precambr. Res. 166 (1–4), 204–218. https://doi.org/10.1016/j.precamres.2007.06.021.

Collins, P.S., 2009. Relinquishment report for EL 23726, for the period 1 August 2003 to 31 July 2009, 801 Project. Open File Company Report, CR2009-0749. https://geoscience.nt.gov.au/gemis/ntgsjspui/handle/1/75417.

Compston, D.M., 1994. Geochronology and evolution of the Tennant Creek Inlier and its ore deposits. Unpublished, Australian National University PhD thesis, Canberra. https://doi.org/10.25911/5d77862d585b0.

Compston, D.M., 1995. Time constraints on the evolution of the Tennant Creek Block, northern Australia. Precambr. Res. 71 (1–4), 107–129. https://doi.org/10.1016/0301-9268(94)00058-Y.

Compston, D.M., McDougall, I., 1994. $^{40}Ar/^{39}Ar$ and K-Ar age constraints on the Early Proterozoic Tennant Creek Block, northern Australia, and the age of its gold deposits. Aust. J. Earth Sci. 41, 609–616. https://doi.org/10.1080/08120099408728171.

Clark, A.D., Highet, L., Schofield, A., Doublier, M., 2021b. Solid Geology map of the East Tennant region. Geoscience Australia, Canberra. http://pid.geoscience.gov.au/dataset/ga/145260.

Clark, A.D., Schofield, A., O'Rourke, A., Doublier, M.P., Roach, I.R., Budd, A.R., Jiang, W., Cross, A., 2021a. Results from the MinEx CRC National Drilling Initiative campaign in East Tennant: What's there and why you should care, Annual Geoscience Exploration Seminar (AGES) Proceedings. Northern Territory Geological Survey, Darwin, 80-83. https://geoscience.nt.gov.au/gemis/ntgsjspui/handle/1/91408.

Crohn, P.W., Oldershaw, W., 1965. The geology of the Tennant Creek one-mile sheet area, Northern Territory. Bureau of Mineral Resources, Geology and Geophysics, Australia, Record 1964/79.
Cross, A.J., Claoué-Long, J.C., Scrimgeour, I.R., Ahmad, M., Kruse, P.D., 2005. Summary of results. Joint NTGS–GA geochronology project: Rum Jungle, basement to southern Georgina Basin and eastern Arunta Region 2001–2003. NTGS Record 2005-006. https://geoscience.nt.gov.au/gemis/ntgsjspui/handle/1/82435.
Cross, A.J., Clark, A.D., Schofield, A., Kositcin, N., 2020. New SHRIMP U-Pb zircon and monazite geochronology of the East Tennant region: a possible undercover extension of the Warramunga Province, Tennant Creek. In: Czarnota, K., Roach, I., Abbott, S., Haynes, M., Kositcin, N., Ray, A., Slatter, E. (Eds.), Exploring for the Future: Extended Abstracts, Geoscience Australia, Canberra, 1–4. https://doi.org/10.11636/132771.
Donnellan, N., 2013. Chapter 9: Warramunga Province. In: Ahmad, M., Munson, T.J. (Eds.), Geology and mineral resources of the Northern Territory, Northern Territory Geological Survey, Darwin. Special Publication 5, 9:1–9:61.
Donnellan, N., Hussey, K.J., Morrison, R.S., 1995. Flynn (5759) and Tennant Creek (5758) 1: 100,000 Geological Map Series. Department of Mines and Energy, Northern Territory Geological Survey.
Donnellan, N., Johnstone, A., 2004. Mapped and Interpreted Geology of the Tennant Region 1:500 000 scale. Northern Territory Geological Survey, Darwin and Alice Springs.
Etheridge, M.A., Rutland, R.W.R., Wyborn, L.A.I., 1987. Orogenesis and tectonic process in the early to middle Proterozoic of northern Australia. Geodynamic series 17. American Geophysical Union, Washington, DC, pp. 131–147.
Farias, P., Cross, A.J., Huston, D.L., 2021. The Rover Field: Insights on stratigraphy, age and base metal mineralisation. In: In: Annual Geoscience Exploration Seminar (AGES) Proceedings, April 2021. Northern Territory Geological Survey, pp. 63–74.
Fletcher, I.R., Davis, W.J., Rayner, N., Orestes Santos, J., 2012. The Moacyr monazite standard: identity and compositional complications. In: 6th International SHRIMP Workshop–Program and Abstracts. Geoscience Australia, Record, Vol. 52, pp. 49–51).
Fraser, G.L., Hussey, K.J., Compston, D.M., 2008. Timing of Palaeoproterozoic Au-Cu-Bi and W-mineralization in the Tennant Creek region, northern Australia: Improved constraints via intercalibration of $^{40}Ar/^{39}Ar$ and U-Pb ages. Precambr. Res. 164 (1–2), 50–65. https://doi.org/10.1016/j.precamres.2008.03.005.
Fraser, G.L., Huston, D.L., Gibson, G.M., Neumann N.L., Maidment, D., Kositcin, N., Skirrow, R.G., Jaireth, S., Lyons, P., Carson, C.J., Cutten, H., Lambeck, A., 2007. Geodynamic and metallogenic evolution of Proterozoic Australia from 1970-1550 Ma, a discussion. Record 2007/16. Geoscience Australia, Canberra. http://pid.geoscience.gov.au/dataset/ga/65342.
Gardner, C.M., 1978. Precambrian geology of the Westmoreland region, northern Australia Part III: Nicholson Granite Complex and Murphy Metamorphics, Bureau of Mineral Resources, Geology and Geophysics, Record 1978/32.
Hanley, L.M., 1996. Geochronology, mineral chemistry, geochemistry and petrology of diamond-associated rocks in the Coanjula Region, Northern Territory. Unpublished University of Western Australia BSc Hons thesis, Perth.
Hill, M., Miller, J., Gallardo, L., 2015. 3D Geological Modelling of the Tennant Creek Region, Northern Territory. Australia. Centre for Exploration Targeting newsletter 55–68.
Holland, T.J.B., Powell, R., 2011. An improved and extended internally consistent thermodynamic dataset for phases of petrological interest, involving a new equation of state for solids. J. Metamorph. Geol. 29, 333–383. https://doi.org/10.1111/j.1525-1314.2010.00923.x.
Hollis, J.A., Beyer, E.E., Whelan, J.A., Kemp, A.I.S., Schersten, A., Greig, A., 2010. Summary of Results. NTGS laser U-Pb and Hf geochronology project: Pine Creek Orogen, Murphy Inlier, McArthur Basin and Arunta Region, June 2007 – June 2008. Northern Territory Geological Survey Record 2010-001. https://geoscience.nt.gov.au/gemis/ntgsjspui/handle/1/82451.
Hollis, J.A., Carson, C.J., Glass, L.M., 2009. SHRIMP U-Pb zircon geochronological evidence for Neoarchean basement in western Arnhem Land, northern Australia. Precambr. Res. 174 (3–4), 364–380. https://doi.org/10.1016/j.precamres.2009.08.010.
Huston, D.L., Cozens, G.J., 1994. The geochemistry and alteration of the White Devil porphyry: implications to intrusion timing. Miner. Deposita 29, 275–287. https://doi.org/10.1007/BF00206871.
Huston, D.L., Cross, A.J., Skirrow, R.G., Champion, D.C., Whelan, J.A., 2020. The Tennant Creek mineral field and Rover fields: Many similarities but some important differences. Annual Geoscience Exploration Seminar (AGES) Proceedings, Northern Territory Geological Survey, Darwin, 70–83. https://geoscience.nt.gov.au/gemis/ntgsjspui/handle/1/90014.
Kelly, E.D., Hoisch, T.D., Wells, M.L., Vervoort, J.D., Beyene, M.A., 2015. An Early Cretaceous garnet pressure–temperature path recording synconvergent burial and exhumation from the hinterland of the Sevier orogenic belt, Albion Mountains Idaho. Contributions Mineral. Petrol. 170, 20. https://doi.org/10.1007/s00410-015-1171-2.
Kositcin, N., Beyer, E.E., Whelan, J.A., Close, D.F., Hallett, L., Dunkley, D.J., 2013. Summary of results. Joint NTGS–GA geochronology project: Arunta Region, Ngalia Basin, Tanami Region and Murphy Province, July 2011–June 2012. Northern Territory Geological Survey Record 2013-004. https://geoscience.nt.gov.au/gemis/ntgsjspui/handle/1/82463.
Kositcin, N., Carson, C.J., 2019. New SHRIMP U–Pb zircon ages from the South Nicholson and Carrara Range region, Northern Territory. Record 2019/09. Geoscience Australia, Canberra. https://doi.org/10.11636/Record.2019.009.
Kositcin, N., Carson, C.J., Anderson, J.R., Doublier, M.P., Murr, J., 2020. Exploring for the Future – New SHRIMP geochronology constraints on the basin evolution of the South Nicholson region. Record 2020/025. Geoscience Australia, Canberra. https://doi.org/10.11636/Record.2020.025.
Kositcin, N., Whelan, J.A., Hallett, L., Beyer, E.E., 2014. Summary of results. Joint NTGS–GA geochronology project: Amadeus Basin, Arunta Region and Murphy Province, July 2012–June 2013. Northern Territory Geological Survey Record 2014-005. https://geoscience.nt.gov.au/gemis/ntgsjspui/handle/1/82466.
Li, Z.X., 2000. Palaeomagnetic evidence for unification of the North and West Australian cratons by *ca.* 1.7 Ga: new results from the Kimberley Basin of northwestern Australia. Geophys. J. Int. 142, 173–180. https://doi.org/10.1046/j.1365-246x.2000.00143.x.
Ludwig, K.R., 2003. User's Manual for Isoplot 3.6 (April 2008 revision). Berkeley Geochronology Center, Special Publication 4. http://sourceforge.net/projects/isoplot/.
Ludwig, K.R., 2009. SQUID 2 Rev. 2.50: A User's Manual. Berkeley Geochronology Center, Special Publication 5. http://sourceforge.net/projects/squid2/.
Maidment, D.W., Houston, D.L., Donnellan, N., Lambeck, A., 2013. Constraints on the timing of the Tennant Event and associated Au–Cu–Bi mineralisation in the Tennant Region, Northern Territory. Precambr. Res. 237, 51–63. https://doi.org/10.1016/j.precamres.2013.07.020.
Maidment, D.W., Lambeck, A., Huston, D.L., Donnellan, N., 2006. New geochronological data from the Tennant Region. Annual Geoscience Exploration Seminar (AGES) Proceedings, Northern Territory Geological Survey, Darwin, 32–35. https://geoscience.nt.gov.au/gemis/ntgsjspui/handle/1/8220.
Maidment, D.W., Wingate, M.T.D., Claoué-Long, J.C., Bodorkos, S., Huston, D.L., Whelan, J.A., Bagas, L., Lambeck, A., Lu, Y., 2020. Geochronology of metasedimentary and granitic rocks in the Granites-Tanami Orogen: 1885–1790 Ma geodynamic evolution. Geological Survey of Western Australia, Report 196, 50p.
McDonald, G.D., Collerson, K.D., Kinny, P.D., 1997. Late Archean and Early Proterozoic crustal evolution of the Mount Isa block, northwest Queensland, Australia. Geology 25 (12), 1095–1098. https://doi.org/10.1130/0091-7613(1997)025<1095:LAAEPC>2.3.CO;2.
McPhie, J., 1993. The Tennant Creek porphyry revisited: A synsedimentary sill with peperite margins, Early Proterozoic, Northern Territory. Aust. J. Earth Sci. 40 (6), 545–558. https://doi.org/10.1080/08120099308728103.
Myers, J.S., Shaw, R.D., Tyler, I.M., 1996. Tectonic evolution of Proterozoic Australia. Tectonics 15 (6), 1431–1446. https://doi.org/10.1029/96TC02356.
Needham, R.S., Stuart-Smith, P.G., Page, R.W., 1988. Tectonic evolution of the Pine Creek Inlier, Northern Territory. Precambr. Res. 40–41, 543–564. https://doi.org/10.1016/0301-9268(88)90084-8.
Neumann, N., Gibson, G., Southgate, P., 2009. New SHRIMP age constraints on the timing and duration of magmatism and sedimentation in the Mary Kathleen Fold Belt, Mt Isa Inlier Australia. Australian J. Earth Sci. 56 (7), 965–983. https://doi.org/10.1080/08120090903005410.
Nguyen, P.T., Booth, S.A., Both, R.A., James, P.R., 1989. The White Devil gold deposit, Tennant Creek, Northern Territory, Australia. Econ. Geol. Monograph 6, 180–192. https://doi.org/10.5382/Mono.06.13.
Orth, K., 2009. Insights into alteration and mineral potential of volcanic succession of the Murphy Inlier and surrounding areas. In: Annual Geoscience Exploration Seminar (AGES) Proceedings, Northern Territory Geological Survey, pp. 32–34.
Page, R.W., Jackson, M.J., Krassay, A.A., 2000. Constraining sequence stratigraphy in north Australian basins: SHRIMP U-Pb zircon geochronology between Mt Isa and McArthur River. Aust. J. Earth Sci. 47 (3), 431–459. https://doi.org/10.1046/j.1440-0952.2000.00797.x.
Palin, R.M., Searle, M.P., Waters, D.J., Parrish, R.R., Roberts, N.M.W., Horstwood, M.S.A., Yeh, M.-W., Chung, S.-L., Anh, T.T., 2013. A geochronological and petrological study of anatectic paragneiss and associated granite dykes from the Day Nui Con Voi metamorphic core complex, North Vietnam: constraints on the timing of metamorphism within the Red River shear zone. J. Metamorph. Geol. 31, 359–387. https://doi.org/10.1111/jmg.2013.31.issue-4.
Payne, J.L., Hand, M., Barovich, K.M., Reid, A., Evans, D.A.D., 2009. Correlations and reconstruction models for the 2500–1500 Ma evolution of the Mawson Continent. Geological Society, London, Special Publications 323, 319–355. https://doi.org/10.1144/SP323.16.
Pearce, M., Gazley, M., White, A., 2014. TC-Investigator: A Matlab Program to Explore Pseudosections. EGU General Assembly, i.d. 14253.
Phillips, C., Orth, K., Hollis, J.A., Kirkland, C.L., Bodorkos, S., Kemp, A.I.S., Wingate, M.T.D., Lu, Y., Iaccheri, L., Page, R.W., 2016. Geology of the Eastern Zone of the Lamboo Province, Halls Creek Orogen, Western Australia. Geol. Surv. Western Australia, Report 164, 57p. http://hdl.handle.net/20.500.11937/56182.
Plumb, K.A., 1979. The tectonic evolution of Australia. Earth-Sci. Rev. 14, 205–249. https://doi.org/10.1016/0012-8252(79)90001-1.
Rattenbury, M.S., 1994. A linked fold-thrust model for the deformation of the Tennant Creek goldfield, northern Australia. Miner. Deposita 29, 301–308. https://doi.org/10.1007/BF00206873.
Rawlings, D.J., Sweet, I.P., Kruse, P.D., 2008. Mount Drummond, Northern Territory. 1: 250 000 geological map series explanatory notes, SE 53-12. Northern Territory Geological Survey, Darwin. https://geoscience.nt.gov.au/gemis/ntgsjspui/handle/1/81809.
Rawlings, D.J., 1999. Stratigraphic resolution of a multiphase intracratonic basin system: the McArthur Basin, northern Australia. Aust. J. Earth Sci. 46, 703–723. https://doi.org/10.1046/j.1440-0952.1999.00739.x.
Rayner, N.M., Stern, R.A., 2002. Improved sample preparation method for SHRIMP analysis of delicate mineral grains exposed in thin sections: in 'Radiogenic Age and Isotope Studies: Report 15' Geol. Survey of Canada. Current Res. 2002–F10.
Schofield, A., Clark, A., Doublier, M.P., Murr, J., Skirrow, R.G., Goodwin, J.A., Cross, A.J., Pitt, L., Duan, J., Jiang, W., Wynne, P., O'Rourke, A., Czarnota, K., Roach, I.C.

2020. Data integration for greenfields exploration: an example from the East Tennant region, Northern Territory. In: Czarnota, K., Roach, I., Abbott, S., Haynes, M., Kositcin, N., Ray, A. and Slatter, E. (eds.) Exploring for the Future: Extended Abstracts, Geoscience Australia, Canberra, 1–4. https://doi.org/10.11636/134444.

Scrimgeour, I.R., 2013. Chapter 12: Aileron Province. In: Ahmad, M., Munson, T.J. (Eds.), Geology and mineral resources of the Northern Territory, Northern Territory Geological Survey, Darwin. Special Publication 5, 12:1–12:74.

Sheppard, S., Tyler, I.M., Griffin, T.J., Taylor, W.R., 1999. Palaeoproterozoic subduction-related and passive margin basalts in the Halls Creek Orogen, northwest Australia. Aust. J. Earth Sci. 46 (5), 679–690. https://doi.org/10.1046/j.1440-0952.1999.00737.x.

Skirrow, R.G., Cross, A.J., Lecomte, A., Mercadier, J., 2019. A shear-hosted Au-Cu-Bi metallogenic event at ~1660 Ma in the Tennant Creek goldfield (northern Australia) defined by in-situ monazite U-Pb-Th dating. Precambrian Res. 332 https://doi.org/10.1016/j.precamres.2019.105402.

Skirrow, R.G., Walshe, J.L., 2002. Reduced and Oxidized Au-Cu-Bi Iron Oxide Deposits of the Tennant Creek Inlier, Australia: An Integrated Geologic and Chemical Model. Econ. Geol. 97 (6), 1167–1202. https://doi.org/10.2113/gsecongeo.97.6.1167.

Smith, J., 2001. Summary of results. Joint NTGS – AGSO age determination program 1999-2001. Northern Territory Geological Survey record 2001-007. https://geoscience.nt.gov.au/gemis/ntgsjspui/handle/1/82409.

Snelling, A.A., Johnston, W.H., 1980. EL 2043 Dalmore Annual Report period ending 28 May 1980, Open File Company Report, CR1980-0157. https://geoscience.nt.gov.au/gemis/ntgsjspui/handle/1/60754.

Stern, R.A., Berman, R.G., 2000. Monazite U-Pb and Th–Pb geochronology by ion microprobe, with an application to in situ dating of an Archean metasedimentary rock. Chem. Geol. 172, 113–130. https://doi.org/10.1016/S0009-2541(00)00239-4.

Stern, R.A., Sanborn, N., 1998. Monazite U–Pb and Th–Pb geochronology by high-resolution secondary ion mass spectrometry. In Radiogenic Age and Isotope Studies: Report 11, 1–18. Geological Survey of Canada Current Research, 1998-F. https://doi.org/10.4095/210049.

Stewart, A.J., Liu, S.F., Highet, L.M., Woods, M., Czarnota, K., Bonnardot, M., Brown, C., Clark, A., Connors, K., 2020. Solid Geology of the North Australian Craton, 1:1 000 000 scale, 1st edition. http://pid.geoscience.gov.au/dataset/ga/135277.

Stipp, M., Stünitz, H., Heilbronner, R., Schmid, S.M., 2002. The eastern Tonale fault zone: A 'natural laboratory' for crystal plastic deformation of quartz over a temperature range from 250 to 700°C. J. Struct. Geol. 24, 1861–1884. https://doi.org/10.1016/S0191-8141(02)00035-4.

Walter, M., Veevers, J., Calver, C., Grey, K., 1995. Neoproterozoic stratigraphy of the Centralian Superbasin, Australia. Precambr. Res. 73 (1–4), 173–195. https://doi.org/10.1016/0301-9268(94)00077-5.

Wedekind, M.R., Large, R.R., Williams, B.T., 1989. Controls on high-grade gold mineralization at Tennant Creek, Northern Territory, Australia. Econ. Geol. Monograph 6, 168–179. https://doi.org/10.5382/Mono.06.12.

Wedekind, M.R., Love, R.J., 1990. Warrego Gold-Copper-Bismuth deposit. In: Hughes, F. E. (Ed.) Geology of the Mineral Deposits of Australia and Papua New Guinea, The Australasian Institute of Mining and Metallurgy, Melbourne, 839–843.

Whelan, J.A., Reno, B.L., Weisheit, A., Kraus, S., Kositcin, N., Woodhead, J.D., Maas, R., Armstrong, R.A., 2017. The geological evolution of the Arnhem Province: implications for craton-scale correlations. In: Annual Geoscience Exploration Seminar (AGES) Proceedings, Northern Territory Geological Survey, pp. 68–73.

Whelan, J.A., Woodhead, J.D., Cliff, J., 2014. Zircon SHRIMP U-Pb, SIMS O and LA-ICPMS Hf isotopic data for granitic gneiss of the Billabong Complex, Tanami Region. Northern Territory Geological Survey, Record 2014-002. https://geoscience.nt.gov.au/gemis/ntgsjspui/handle/1/82465.

White, R.W., Powell, R., Holland, T.J.B., Johnson, T.E., Green, E.C.R., 2014. New mineral activity–composition relations for thermodynamic calculations in metapelitic systems. J. Metamorph. Geol. 32, 261–286. https://doi.org/10.1111/jmg.12071.

Worden, K.E., Carson, C.J., Scrimgeour, I.R., Lally, J., Doyle, N., 2008. A revised Palaeoproterozoic chronostratigraphy for the Pine Creek Orogen, northern Australia: Evidence from SHRIMP U-Pb zircon geochronology. Precambr. Res. 166, 122–144. https://doi.org/10.1016/j.precamres.2007.05.009.

Wyborn, L.A.I., Budd, A.R., Bastrakova, I.V., 1998. Metallogenic potential of the felsic igneous rocks of the Tennant Creek and Davenport Provinces, Northern Territory. AGSO Res. Newsl. 29, 26–28.

Wyborn, L.A.I., Page, R.W., Parker, A.J., 1987. Geochemical and geochronological signatures in Australian Proterozoic igneous rocks. In: Pharaoh, T.C., Beckinsale, R. D., Rickard, D. (Eds.), Geochemistry and Mineralization of Proterozoic Volcanic Suites, Geol. Soc. Special Publication 33, 377–394. https://doi.org/10.1144/GSL.SP.1987.033.01.26.

Zhao, J.-X., Cooper, J.A., 1992. The Atnarpa Igneous Complex, southeast Arunta Inlier, central Australia: implications for subduction at an Early-Mid Proterozoic continental margin. Precambr. Res. 56 (3–4), 227–253. https://doi.org/10.1016/0301-9268(92)90103-U.

Zhao, G., Sun, M., Wilde, S.A., Li, S., 2004. A Paleo-Mesoproterozoic supercontinent: assembly, growth and breakup. Earth Sci. Rev. 67 (1–2), 91–123. https://doi.org/10.1016/j.earscirev.2004.02.003.